Optogenetic astrocyte activation evokes BOLD fMRI response with oxygen consumption without neuronal activity modulation

Journal:	*GLIA*
Manuscript ID	GLIA-00462-2017.R2
Wiley - Manuscript type:	Original Research Article
Date Submitted by the Author:	n/a
Complete List of Authors:	Takata, Norio; Keio Univ. Sch. of Med., Neuropsychiatry; Central Institute for Experimental Animals (CIEA) Sugiura, Yuki; Keio Univ. Sch. of Med., Biochemistry Yoshida, Keitaro; Keio Univ. Sch. of Med., Neuropsychiatry Koizumi, Miwako; Keio Univ. Sch. of Med., Neuropsychiatry Hiroshi, Nishida; Keio Univ. Sch. of Med., Neuropsychiatry Honda, Kurara; Keio Univ. Sch. of Med., Biochemistry Yano, Ryutaro; Keio University School of Medicine, Physiology Komaki, Yuji; Central Institute for Experimental Animals (CIEA) Matsui, Ko; Tohoku University, Graduate School of Life Sciences Suematsu, Makoto; Keio Univ. Sch. of Med., Biochemistry Mimura, Masaru; Keio Univ. Sch. of Med., Neuropsychiatry Okano, Hideyuki; Keio Univ. Sch. of Med., Physiology; RIKEN Brain Science Institute Tanaka, Kenji ; Keio University School of Medicine, Neuropsychiatry
Key Words:	astrocytes, optogenetics, BOLD, fMRI, imaging mass spectrometry

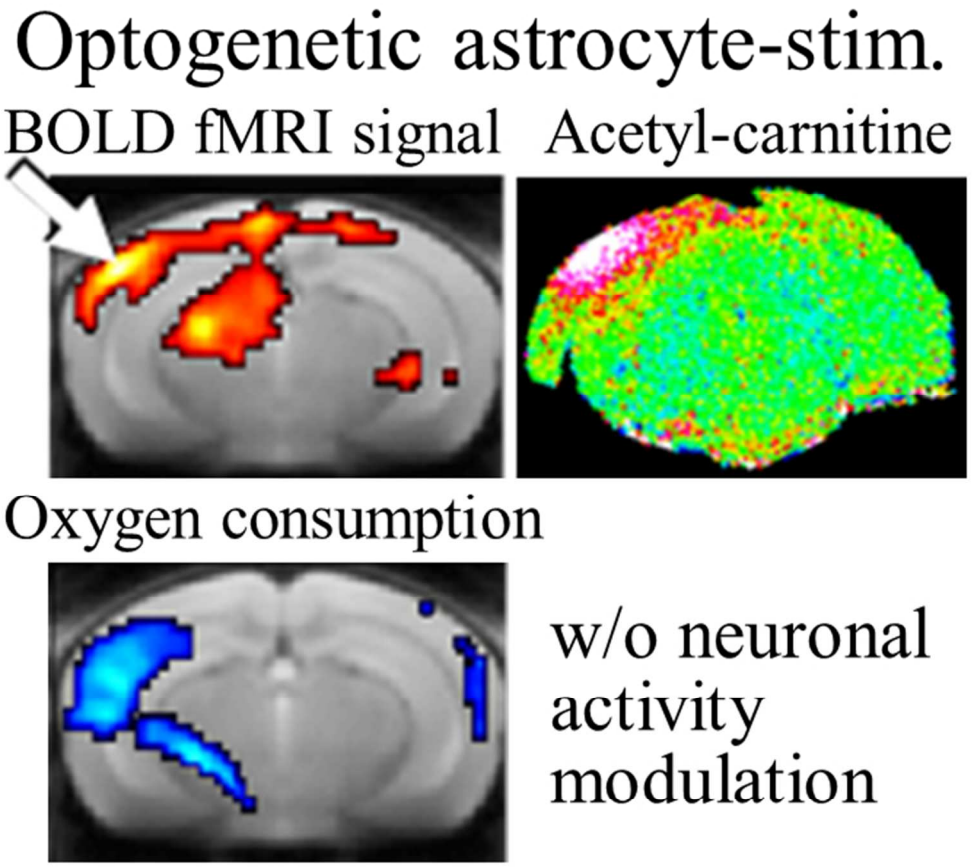

Table of Contents Image (TOCI)

58x52mm (300 x 300 DPI)

Optogenetic astrocyte activation evokes BOLD fMRI response with oxygen consumption without neuronal activity modulation

Running title: Astrocytes evoke BOLD fMRI response

Norio Takata[a,b], Yuki Sugiura[c], Keitaro Yoshida[a], Miwako Koizumi[a], Hiroshi Nishida[a], Kurara Honda[c], Ryutaro Yano[d], Yuji Komaki[b], Ko Matsui[e], Makoto Suematsu[c], Masaru Mimura[a], Hideyuki Okano[d,f], Kenji F. Tanaka[a]

a. Department of Neuropsychiatry, Keio University School of Medicine, 35 Shinanomachi, Shinjuku, Tokyo 160-8582, Japan
b. Central Institute for Experimental Animals (CIEA), 3-25-12, Tonomachi, Kawasaki, Kanagawa 210-0821, Japan
c. Department of Biochemistry, Keio University School of Medicine, 35 Shinanomachi, Shinjuku, Tokyo 160-8582, Japan
d. Department of Physiology, Keio University School of Medicine, 35 Shinanomachi, Shinjuku, Tokyo 160-8582, Japan
e. Super-network Brain Physiology, Graduate School of Life Sciences, Tohoku University, Sendai, Miyagi 980-8575, Japan
f. Laboratory for Marmoset Neural Architecture, RIKEN Brain Science Institute, Wako, Saitama 351-0198, Japan

Corresponding Authors

Norio Takata, Ph.D. Email: takata.norio@keio.jp
Kenji F. Tanaka, M.D., Ph.D. Email: kftanaka@keio.jp
Department of Neuropsychiatry, Keio University School of Medicine,
35 Shinanomachi, Shinjuku, Tokyo, 160-8582, Japan
Tel +81-3-5363-3934;

Acknowledgements

We thank Dr. Kouichi C. Nakamura for a generous gift of an antibody. We also thank Dr. Youcef Bouchekioua for his technical support. This work was supported by Takeda Science Foundation to N.T.; JSPS KAKENHI Grant Numbers (25430011, 25115726, 15KT0111, 16H01620, and 16K07032 to N.T., 24111551 and 26290021 to K.F.T.); Brain/MINDS and the Strategic Research Program for Brain Sciences (SRPBS) from the Ministry of Education, Culture, Sports, Science, and Technology of Japan (MEXT) and Japan Agency for Medical Research and Development (AMED) to N.T., K.F.T. and H.O..

Word Count

Total word count: 7382 (Abstract: 149, Introduction: 593, Materials and Methods: 215, Results: 2175, Discussion: 998, References: 1910, Figure Legends: 987.)

Number of Pages: 33

Number of Tables: 0; Total number of figures: 4; Number of Color Images: 4

Table of Contents

Main Points

--- Optogenetic activation of astrocytes evoked BOLD signal that accompanied oxygen consumption without modulation of neuronal activity.

--- Acetyl-carnitine was synthesized at the site of astrocyte-, but not neuron-evoked BOLD signal.

47 # Table of Contents Image (TOCI)

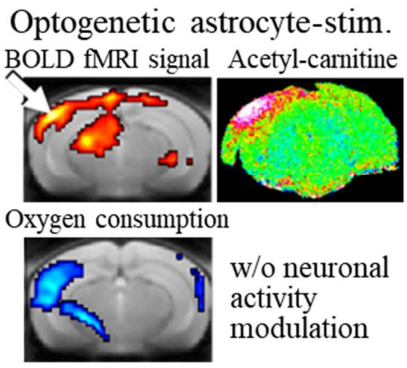

48

Abstract

Functional magnetic resonance imaging (fMRI) based on the blood oxygenation level-dependent (BOLD) signal has been used to infer sites of neuronal activation in the brain. A recent study demonstrated, however, unexpected BOLD signal generation without neuronal excitation, which led us to hypothesize the presence of another cellular source for BOLD signal generation. Collective assessment of optogenetic activation of astrocytes or neurons, fMRI in awake mice, electrophysiological measurements, and histochemical detection of neuronal activation, coherently suggested astrocytes as another cellular source. Unexpectedly, astrocyte-evoked BOLD signal accompanied oxygen consumption without modulation of neuronal activity. Imaging mass spectrometry of brain sections identified synthesis of acetyl-carnitine via oxidative glucose metabolism at the site of astrocyte-, but not neuron-evoked BOLD signal. Our data provide causal evidence that astrocytic activation alone is able to evoke BOLD signal response, which may lead to reconsideration of current interpretation of BOLD signal as a marker of neuronal activation.

Keywords

astrocytes; BOLD; optogenetics; fMRI; imaging mass spectrometry

Introduction

Blood oxygenation level-dependent (BOLD) functional magnetic resonance imaging (fMRI) is a fundamental imaging tool in basic and clinical investigations of human brain activity (Ogawa, Lee, Kay, & Tank, 1990). The BOLD signal is not a direct measurement of neuronal activity; instead, the signal is influenced by cerebral blood flow (CBF), cerebral blood volume (CBV), and the cerebral metabolic rate of oxygen consumption (Ogawa, Menon, Kim, & Ugurbil, 1998; Shen, Ren, & Duong, 2008). Despite the above caveats, the BOLD signal has been widely used as a surrogate marker of neuronal activation, because accumulating evidence has demonstrated a close correlation between BOLD signal response and electrophysiological activation of neurons following sensory stimulation (Logothetis, Pauls, Augath, Trinath, & Oeltermann, 2001; Niessing et al., 2005). Recent optogenetic fMRI (ofMRI) studies have further confirmed the correlation (Kahn et al., 2013; Lee et al., 2010; Takata et al., 2015). However, the cellular mechanisms of BOLD signal generation have not been fully elucidated (Ekstrom, 2010; Vanzetta & Slovin, 2010). It is reported that coupling between BOLD and electrophysiological signal in visual cortex of behaving monkeys is context dependent (Maier et al., 2008). Furthermore, unexpected BOLD signal generation is found without activation of local neurons in the visual cortex of monkeys performing a fixation-on-off task (Sirotin & Das, 2009).

Astrocytes are also considered to participate in BOLD signal generation (Haydon & Carmignoto, 2006; Otsu et al., 2015; Schummers, Yu, & Sur, 2008; Takano et al., 2006), but in a passive way that just couples neuronal activity to the hemodynamic

response to fulfill metabolic demand of neurons (Petzold & Murthy, 2011; Raichle & Mintun, 2006). A study that combined BOLD fMRI and fiber-optic calcium (Ca^{2+}) recording in the cortex of anesthetized rats during electrical paw stimulation reported a correlation between prolonged BOLD signal components and Ca^{2+} surge in astrocytes, and their modeling suggested involvement of astrocytes in a late component of the BOLD response (Schulz et al., 2012). However, direct investigation of causal relationship between astrocyte activation and BOLD signal generation seems difficult to examine in the study, because sensory stimulation inevitably activates neurons in addition to astrocytes. Moreover, a recent study reported intact BOLD signal response upon hindpaw stimulation of anesthetized inositol 1,4,5-triphosphate receptor type 2 knock-out (IP_3R2-KO) mice, which lack large cytosolic Ca^{2+} surges in astrocytes, suggesting a minor role of astrocytic Ca^{2+} activity in BOLD signal generation (Jego, Pacheco-Torres, Araque, & Canals, 2014) (but see (Srinivasan et al., 2015; Stobart et al., 2016) that demonstrate preserved Ca^{2+} dynamics in astrocytes of IP_3R2-KO mice, and (Mishra et al., 2016) that shows multiple sources of calcium signals in astrocytes). Note that most of these studies were performed under anesthesia, which could affect neurovascular coupling, energy metabolism, and BOLD signal generation (Masamoto & Kanno, 2012; Sokoloff et al., 1977).

This study aimed to investigate a causal relationship between astrocyte activity and BOLD signal generation using ofMRI in awake transgenic mice, whose cortical neurons or astrocytes express channelrhodopsin-2 (ChR2) (Tanaka et al., 2012). Optical activation of either neurons or astrocytes by light illumination through intact skull evoked a BOLD signal response in the cortex. Oxygen consumption upon stimulation of

either neurons or astrocytes was suggested by experiments of ofMRI in the presence of a vasodilator. Unexpectedly, optical activation of astrocytes did not modulate neuronal activity, which was confirmed with *in situ* hybridization for *c-fos* mRNA and *in vivo* electrophysiology. Metabolic underpinnings of the oxygen consumption was investigated with metabolite imaging of brain sections using imaging mass spectrometry (IMS). Activation of astrocytes, but not neurons, augmented synthesis of acetyl-carnitine (AC) from glucose, which consumed oxygen. Collectively, our findings demonstrate unexpected active role of astrocytes in BOLD signal generation.

Materials and Methods

fMRI in awake mice.

We have elaborated fMRI in awake mice using a high signal-to-noise ratio cryogenic MRI detector, CryoProbe (Yoshida et al., 2016). Confounding effects of anesthetics during fMRI in awake mice were avoided because anesthesia is not necessary with this protocol to place awake mice in an animal bed of MRI.

In vivo multichannel extracellular recordings.

Extracellular recording was performed as described previously (Takata et al., 2015). A 16-channel, linear silicon probe was inserted through a craniotomy (Φ 0.5 mm; AP -3.0 mm, ML -2.0 mm) for recording from the cortex, which corresponds to the site of global peak of BOLD signal response upon optogenetic astrocyte activation (Fig. 2c).

IMS with FMW-assisted brain fixation for $^{13}C_6$-glucose metabolic pathway tracing.

Two-dimensional imaging of metabolites in the brain slices by combining IMS,

FMW, and ^{13}C-isotope was reported previously (Sugiura, Honda, Kajimura, & Suematsu, 2014; Sugiura, Taguchi, & Setou, 2011). To trace the metabolic fate of glucose, $^{13}C_6$-glucose was injected intraperitoneally. Fifteen minutes later (Sugiura et al., 2014), optogenetic stimulation of the left cortex through the intact skull was performed. Thirty seconds later, mice were euthanized by FMW-irradiation for 0.96 s on the brain (Sugiura, Honda, & Suematsu, 2015). Matrix-assisted laser desorption ionization (MALDI)-IMS was performed on thin sections of the brain. See Supplementary Materials and Methods for more details.

Results

Transcranial illumination of the cortex of awake mice that express ChR2(C128S) in neurons or astrocytes.

Double transgenic animals that express ChR2(C128S), a step-function opsin-type variant of ChR2 (Berndt, Yizhar, Gunaydin, Hegemann, & Deisseroth, 2009), were generated by crossing a tetO-ChR2(C128S)-YFP line with a cell-type specific-tTA line (Tanaka et al., 2012); hereafter, we refer to *Chrm4*-tTA::tetO-ChR2(C128S)-YFP and *Mlc1*-tTA::tetO-ChR2(C128S)-YFP double transgenic lines as Neuron-ChR2 and Astrocyte-ChR2, respectively. For gene manipulation strategies to generate transgenic mice, see Supplementary Fig. 1. Expression of ChR2(C128S)-EYFP was observed in the cortex and sub-cortical brain structures of both Neuron- and Astrocyte-ChR2 mice (Fig. 1a, d). Double immunostaining for NeuN (neuron marker) and YFP (ChR2-marker) showed high expression levels of ChR2(C128S) at neuronal somas in layer IV and at dendrites in layer

159 II/III of the cortex of Neuron-ChR2 mice (Fig. 1b, c). In Astrocyte-ChR2 mice, almost
160 uniform expression of ChR2(C128S) was observed throughout the cortical layers (Fig.
161 1e). The enlarged view of the staining reveals the expression pattern of ChR2(C128S)
162 with fine laminar morphology that is characteristic of astrocytes (Fig. 1f). Moreover, we
163 have shown co-expression of ChR2(C128S) and GLAST, an astrocyte specific glutamate
164 transporter, in the brain of Astrocyte-ChR2 mice (Tanaka et al., 2012), further
165 confirming astrocytic expression of ChR2(C128S). Expression of ChR2(C128S) across a
166 wide cortical area in these transgenic mice lines allows transcranial manipulation of
167 neuronal or astrocytic activity because ChR2(C128S) has higher sensitivity than
168 conventional ChR2 (Mattis et al., 2012).

169 To perform light illumination through the intact skull of awake mice during
170 fMRI experiments, a skull-holder and an optic fiber were attached horizontally on the
171 skull (Yoshida et al., 2016). fMRI on awake mice is advantageous to avoid the
172 confounding effects of anesthetics on neuronal and astrocytic activity (Greenberg,
173 Houweling, & Kerr, 2008; Thrane et al., 2012). The tip of an optic fiber was
174 positioned on the intact skull over the left visual cortex (Fig. 1g, h, i).

175 Optogenetic stimulation of astrocytes as well as
176 neurons evokes BOLD signal response.

177 We investigated whether transcranial photo-activation of neurons or astrocytes
178 was able to induce a BOLD signal response using Neuron- or Astrocyte-ChR2 mice,
179 respectively. Transcranial manipulation is desirable to avoid inserting an optic fiber into
180 the brain, which may result in “reactive astrocytes” with distinct physiological
181 characteristics (Aguado, Espinosa-Parrilla, Carmona, & Soriano, 2002). We

applied a pair of blue and yellow lights with 30 s separation, which kept a cation channel of ChR2(C128S) open for 30 s. This pair of lights was repeated 3 times at an interval of 2 min. The duration of each light was 0.5 and 5.0 s for Neuron- and Astrocyte-ChR2 mice, respectively. We employed longer illumination in Astrocyte-ChR2 mice because we speculated that effect of optogenetic stimulation was smaller in astrocytes, considering that astrocytic membrane resistance is lower than neurons.

We found that transcranial optogenetic stimulation of either neurons or astrocytes could evoke a BOLD signal response in the cortex (Fig. 2a, c). The response was observed dominantly in the left cortex, which was ipsilateral to the site of light illumination. The most significant BOLD signal response was evoked within the cortex of Neuron- and Astrocyte-ChR2 mice (arrows in Fig. 2a, c). Subcortical BOLD signal response may reflect direct photo-activation, based on our measurements of ofMRI using a triple transgenic mouse whose astrocytes express ChR2(C128S) except in the cortex (see Supplementary Results and Supplementary Fig. 2a-d). In addition, light illumination for optogenetic stimulation seemed not enough to evoke BOLD signal response through visual stimulation nor brain-tissue heating (see Supplementary Results and Supplementary Fig. 3a, b). Further, open field test and ofMRI using *anesthetized* Astrocyte-ChR2 mice suggested that behavioral state-change, which may cause widespread astrocyte excitation in the brain, seemed not to contaminate BOLD signal fluctuation upon optogenetic stimulation of astrocytes (see Supplementary Results, Supplementary Fig. 2e, f, and Supplementary Fig. 4).

We compared temporal dynamics of BOLD signal fluctuations at the site of the most significant response upon optogenetic stimulation of Neuron- or Astrocyte-ChR2

mice, respectively (arrows in Fig. 2a, c). A BOLD signal response could be evoked repeatedly in both Neuron- and Astrocyte-ChR2 mice (Fig. 2b, d). Peak amplitudes of the response during the first stimulation period, i.e., 30 s-period between a pair of blue and yellow vertical lines (Fig. 2b, d), were significantly higher for Neuron- than Astrocyte-ChR2 mice (6.1 ± 0.4% versus 4.7 ± 0.5%, $P = 0.03$, n = 12 and 9 animals for Neuron- and Astrocyte-ChR2 mice, respectively; two-sample *t*-test). The magnitude of the BOLD signal response was dependent on the light intensities (Supplementary Fig. 3c, d).

Oxygen consumption is elicited by optogenetic stimulation of either astrocytes or neurons.

Because BOLD signal has been considered to reflect augmentation of the metabolic demand of neurons (Heeger & Ress, 2002), we addressed whether astrocyte-evoked BOLD signal response resulted in oxygen consumption. We performed ofMRI after injection of a nitric oxide-releasing vasodilator, sodium nitroprusside (SNP), so that oxygen consumption could be detected as negative deflection of the BOLD signal (Nagaoka et al., 2006).

Neuronal activation by optogenetic stimulation using Neuron-ChR2 mice in the presence of SNP resulted in a negative BOLD response (Fig. 2e, f), which was in good accordance with previous studies (Nagaoka et al., 2006; Tsurugizawa, Ciobanu, & Le Bihan, 2013). The location of the most significant negative BOLD signal was similar to that of the positive BOLD response in ofMRI experiments without SNP (compare arrows in Fig. 2a and e). The negative deflection of the BOLD signal occurred only once, followed by a gradual increase that exceeded baseline (Fig. 2f) (see below).

Astrocyte activation by optogenetic stimulation using Astrocyte-ChR2 mice in the presence of SNP also resulted in a negative BOLD response (Fig. 2g, h), which suggests that activation of astrocytes results in oxygen consumption. The location of the most significant negative BOLD signal was comparable to that of the positive BOLD response in ofMRI experiments without SNP (compare arrows in Fig. 2c and g). Negative deflection of the BOLD response was observed only once to the first optogenetic stimulation of astrocytes (Fig. 2h), which was similar to the result in Neuron-ChR2 mice (Fig. 2f), although the gradual increase of the BOLD signal after the first optogenetic stimulation was not as clear as that in Neuron-ChR2 mice.

It's not clear in this study why negative deflection was hardly induced by the second and the third illumination on Neuron- or Astrocyte-ChR2 mice. BOLD signal is assumed to reflect increase of 1) blood volume, 2) blood flow, and 3) oxygenation in the blood (Shen et al., 2008). Considering that SNP suppresses the first two factors, gradual increase of BOLD signals might indicate physiological response to suppress oxygen consumption in the brain in the presence of SNP after the first optical stimulation. This might explain the absence of negative BOLD response upon the second and the third illumination.

Neuronal activation is not observed by optogenetic stimulation of astrocytes.

Because BOLD signal is used as a marker of neuronal activation, we examined the modulation of neuronal activity upon optogenetic stimulation of Neuron- or Astrocyte-ChR2 mice. We first performed *in situ* hybridization for *c-fos* mRNA, a neuronal activity marker, to obtain the spatial distribution of neuronal activation. Animals were perfused 30 min after optogenetic stimulation, and then post-fixed, sliced, and

252 stained for *c-fos* mRNA.

253 Neuronal activation of Neuron-ChR2 mice increased *c-fos* mRNA staining in the
254 ipsilateral cortex to the site of light illumination (Fig. 3a), which is consistent with
255 previous reports (Stark, Davies, Williams, & Luckman, 2006). Unexpectedly,
256 astrocyte activation of Astrocyte-ChR2 mice did not augment *c-fos* mRNA staining (Fig.
257 3b). We quantified staining intensity for *c-fos* mRNA in the left and right cortex (blue and
258 red rectangles in Fig. 3a, b, respectively) by calculating their mean pixel values. While
259 Neuron-ChR2 mice showed significantly higher staining for *c-fos* mRNA in the left
260 cortex than that in the right cortex (107 ± 3 versus 83 ± 7 in the left and right cortex, P =
261 0.02, n = 9 mice, paired *t*-test; Fig. 3a), Astrocyte-ChR2 mice showed comparable
262 staining for *c-fos* mRNA in the left and right cortex (79 ± 6 versus 79 ± 6 in the left and
263 right cortex, P = 0.86, n = 9 mice, paired *t*-test; Fig. 3b).

264 This result cannot distinguish the following possibilities: 1) optogenetic
265 activation of astrocytes indeed did not modulate neuronal activity, or 2) it did modulate
266 neuronal activity, but was not enough to increase expression of *c-fos* mRNA. To directly
267 examine neuronal activity upon optogenetic stimulation of neurons or astrocytes, we next
268 performed electrophysiological recording in the cortex of awake, head-fixed Neuron- or
269 Astrocyte-ChR2 mice, using a linear 16-channel silicon probe electrode. This was a
270 separate experiment to the ofMRI. Again, we observed neuronal activation upon
271 optogenetic stimulation of Neuron-, but not of Astrocyte-ChR2 mice (Fig. 3c-f),
272 supporting the first possibility.

273 Specifically, in Neuron-ChR2 mice, local field potential (LFP) power at the
274 gamma and high frequency oscillation (HFO) significantly increased at the beginning of

the stimulation, followed by a gradual decrease (Fig. 3c). Average power of LFP at gamma and HFO during the period of the first light-activation was significantly higher than that during the pre-stimulus period (bar graph at lower right of Fig. 3c; 6.3 ± 1.2 and 2.0 ± 0.6 for gamma and HFP; $P = 0.003$ and 0.02, respectively; n = 6 mice, paired *t*-test). Multi-unit activities (MUA) in the cortex were also augmented by the optogenetic stimulation of Neuron-ChR2 mice (Fig. 3e). The mean relative number of spikes during the first activation period (60~90 s) was significantly higher than that during the pre-stimulus period (lower panel of Fig. 3e; 3.4 ± 0.6, $P = 0.01$, n = 6 mice, paired *t*-test). These results are in good accordance with previous reports (Kahn et al., 2013; Lee et al., 2010; Takata et al., 2015).

In Astrocyte-ChR2 mice, optogenetic activation of astrocytes did not modulate LFP power (Fig. 3d). The average power of LFP during the first light activation period was not different from that during the pre-stimulus period (bar graph at lower right of Fig. 3d; -0.2 ± 0.3, -0.5 ± 0.4, -0.4 ± 0.4, and -0.1 ± 0.3 for delta, theta, gamma, and HFO, respectively, $P > 0.25$, n = 5 mice, paired *t*-test). Neither was MUA modulated (mean relative number of spikes during the first activation period: 1.3 ± 0.2, $P = 0.22$, n = 5 mice, paired *t*-test).

Illumination using only yellow light did not evoke electrophysiological response in Neuron- or Astrocyte-ChR2 mice (Supplementary Fig. 5a–d). The magnitude of electrophysiological response was dependent on intensities of blue light (Supplementary Fig. 5e–h). These results were consistent with that of ofMRI (Supplementary Fig. 3).

$^{13}C_6$-glucose is metabolized into $^{13}C_2$-AC by optogenetic activation of astrocytes, but not neurons.

We asked whether neuron- or astrocyte-evoked BOLD signal was underlain by the same metabolic activity because astrocyte-evoked BOLD signal accompanied oxygen consumption without neuronal activation (Fig. 2 and 3). We used IMS to examine two-dimensional distribution of brain metabolites upon optogenetic stimulation of Neuron- or Astrocyte-ChR2 mice (n = 3 and 5 mice, respectively). Intraperitoneal injection of ^{13}C-isotope labeled glucose ($^{13}C_6$-glucose) was performed fifteen minutes before optogenetic stimulation, which allowed us to trace flows of ^{13}C from glucose to various metabolites (Fig. 4a, b). Transcranial light illumination for optogenetic stimulation of neurons or astrocytes was executed as before. Thirty seconds after the stimulation, focused microwave (FMW) irradiation was applied for 0.92 s to the head of the mouse to rapidly inactivate enzymatic reactions in the brain, which minimizes postmortem alterations in metabolites during brain extraction (Sugiura et al., 2015). Brains were then extracted, frozen, and sliced coronally at a thickness of 8 μm. The spatial distribution of ^{13}C-containing metabolites that were synthesized from $^{13}C_6$-glucose was explored and visualized using IMS.

Optogenetic stimulation of astrocytes, but not neurons, resulted in an increase of non-labeled AC and $^{13}C_2$-AC at the site of light illumination in the cortex (Fig. 4c and d, middle row), suggesting that AC was metabolized from glucose via oxidative decarboxylation of pyruvate to produce acetyl-CoA followed by transfer of acetyl-group to carnitine (Fig. 4b). Concomitantly, reduction of carnitine, a substrate for AC synthesis, was observed at the same region in the brain of Astrocyte-ChR2 mice (dotted circles in Fig. 4d, upper right panel), indicating that synthesis of AC from acetyl-CoA and carnitine

320 occurred in the brain. Spatial patterns of fluctuation of these metabolites were similar to
321 that of the BOLD signal response upon astrocyte activation (compare Fig. 2c with the
322 bottom panels of Fig. 4d or Supplementary Fig. 6a), implying that astrocyte activation
323 accelerated the metabolic pathway that produces AC in the brain. Notably, optogenetic
324 stimulation of astrocytes did not result in accumulation of NADH (Supplementary Fig. 6b,
325 upper right panel). This suggests the presence of oxidative conversion of NADH to NAD^+
326 by mitochondrial complex I activity (Fig. 4b). These imaging results were also supported
327 by a capillary electrophoresis (CE)-electrospray ionization (ESI)-mass spectrometry
328 (MS) technique (Morikawa et al., 2012; Sugiura et al., 2016) (Supplementary Fig.
329 7). Taken together, these results suggest that while comparable a BOLD signal response
330 was evoked by optogenetic stimulation of either neurons or astrocytes, the respective
331 BOLD signal fluctuations were accompanied by distinct metabolic flows.
332

333 Discussion

334 We demonstrated that 1) selective stimulation of astrocytes is sufficient for the
335 induction of a BOLD signal response with oxygen consumption in the absence of
336 neuronal activation, and 2) activation of astrocytes, but not neurons, resulted in glucose
337 oxidation with production of AC, which is known to modulate neuronal energy processes
338 (Pettegrew, Levine, & McClure, 2000; Traina, 2016). Our data present a causal
339 relationship between astrocyte activation and BOLD signal generation, suggesting that
340 BOLD signal fluctuations can reflect metabolic demands of astrocytes in addition to
341 neurons. These findings may challenge the current interpretation of the BOLD signal
342 response as a surrogate marker of neuronal activation in fMRI studies (Figley &

343 Stroman, 2011; Gurden, 2013).

344 The physiological relevance of optogenetic stimulation of astrocytes has not
345 been resolved completely, while increasingly many studies have recently employed
346 optogenetic manipulation of astrocytes to utilize its advantages to shift the states of
347 astrocytes non-invasively with cell-type specificity (Figueiredo et al., 2014; Gourine
348 et al., 2010; Masamoto et al., 2015; Pelluru, Konadhode, Bhat, & Shiromani,
349 2016; Perea, Yang, Boyden, & Sur, 2014; Sasaki et al., 2012; Tanaka et al.,
350 2012; Tang et al., 2014). The responses of astrocytes upon optogenetic activation have
351 been reported as a few mV of depolarization, pH decrease, and cytosolic Ca^{2+} surge
352 (Beppu et al., 2014; Perea et al., 2014; Sasaki et al., 2012), which can be
353 observed in physiological situations (MacVicar, Crichton, Burnard, & Tse, 1987; Rose &
354 Ransom, 1996; Seigneur, Kroeger, Nita, & Amzica, 2006; Takata et al., 2011).

355 Among the above three responses, depolarization of astrocytes might be the
356 primary cause for BOLD signal induction in the current study, because we reported
357 previously that astrocytic depolarization was coupled to efflux of potassium ions, a potent
358 vasodilator, from astrocytes (Masamoto et al., 2015; Sasaki et al., 2012). Although we
359 have shown that only ~5 mV depolarization was evoked with significantly larger light
360 power (7 mW/mm^2 blue light illumination for 10 s; see Supplementary Materials and
361 Methods) on Bergmann glial cells (astrocytes in the cerebellum) in slice preparation from
362 young Astrocyte-ChR2 mice (postnatal day 17 to 24), we have also demonstrated that
363 amplitude of optogenetically induced inward currents developed age-dependent manner
364 (Sasaki et al., 2012), suggesting that effect of optogenetic stimulation is larger in the
365 current study that uses adult Astrocyte-ChR2 mice.

In the current study, optogenetic stimulation of astrocytes did not significantly activate neurons, which may appear inconsistent with previous reports that showed induction of *c-fos* mRNA in neuronal and/or glial cells upon optogenetic activation of astrocytes in the cortex or cerebellum using Astrocyte-ChR2 mice (Sasaki et al., 2012; Tanaka et al., 2012). While light intensity at the tip of the optic fiber was comparable among studies, the layout of the optic fiber differed: earlier studies placed an optic fiber perpendicular to the cranial skull, while the fiber was placed horizontally in the present study. Thus, it is conceivable that less light reached the brain in the current study, which may explain the lack of modulation of neuronal activity upon optogenetic manipulation of astrocytes. In line with this, astrocytes show distinct physiological response depending on stimulation intensity (Sekiguchi et al., 2016). It is possible that previous studies employed light illumination that was strong enough to modulate neuronal activity, because most of the studies used neuronal response as a readout for optogenetic manipulation of astrocytes. It should be noted, however, that axonal activity cannot be detected with our extracellular electrodes. Therefore, the current study cannot exclude a possibility that optogenetic manipulation of astrocytes might have modulated axonal activity (Tang et al., 2014), which may lead to BOLD signal generation. Note that even in this case, our results support the idea of causal involvement of astrocytes in BOLD signal generation.

Optogenetic stimulation of astrocytes resulted in unexpected oxygen consumption without neuronal activation. We have previously shown that optogenetic activation of astrocytes results in potassium efflux from astrocytes (Masamoto et al., 2015), which should be followed by restoration of the ionic gradient of astrocytes by

389 Na^+-/K^+-ATPase. Thus, synthesis of adenosine triphosphate (ATP) might be a candidate
390 to account for the oxygen consumption, although we did not observe a significant
391 increase in ATP upon optogenetic stimulation of astrocytes (Supplementary Fig. 6). AC
392 might be another candidate for oxygen consumption upon optogenetic astrocyte
393 activation, because metabolism from glucose to AC involves production of NADH, an
394 electron donor that transfers an electron to molecular oxygen during oxidative
395 phosphorylation in mitochondria (Fig. 4b). In accord with this idea, NADH was not
396 accumulated (Supplementary Fig. 6) while AC synthesis was evident (Fig. 4d) upon
397 optogenetic stimulation of astrocytes, suggesting consumption of a molecular oxygen by
398 oxidization of NADH to NAD^+ in mitochondria (Fig. 4b). See Supplementary Discussion
399 on the possibility of AC as an energy substrate for neurons.
400 The BOLD signal response has been used to infer activation of neurons because
401 accumulating evidence has shown a close correlation between BOLD signal fluctuations
402 and electrophysiological activation of neurons (Logothetis et al., 2001; Niessing et
403 al., 2005). However, in the present study, we demonstrated that astrocytes can evoke a
404 BOLD signal response that accompanies oxygen consumption without activation of local
405 neurons. This may suggest the existence of BOLD signal fluctuations that are irrelevant
406 to activation of local neurons. Indeed, a recent study found unexpected BOLD signal
407 fluctuations that occurred without activation of local neurons during a repeated
408 anticipation task (Sirotin & Das, 2009). Activation of astrocytes might be a cellular
409 substrate underlying this type of BOLD signal fluctuation. What physiological
410 mechanism might stimulate astrocytes without activation of local neurons? One
411 possibility might be the release of neuromodulator(s) from axonal fibers of distant origin.

412 It's shown that astrocytes are sensitive to neuromodulators such as acetylcholine and
413 noradrenalin, which can be released in the cortex by axonal fibers ascending from the
414 Meynert nucleus or Locus coeruleus, respectively (Bekar, He, & Nedergaard, 2008;
415 Pankratov & Lalo, 2015; Takata et al., 2011). Thus, astrocytes may be able to
416 respond to neuromodulatory activity of remote neurons, by augmenting metabolic
417 activity including synthesis of AC that can be used as preparatory energy fuel for local
418 neurons.

References

Aguado, F., Espinosa-Parrilla, J. F., Carmona, M. A., & Soriano, E. (2002). Neuronal activity regulates correlated network properties of spontaneous calcium transients in astrocytes in situ. *The Journal of Neuroscience*, *22* (21), 9430–9444.

Bekar, L. K., He, W., & Nedergaard, M. (2008). Locus coeruleus alpha-adrenergic-mediated activation of cortical astrocytes in vivo. *Cerebral Cortex*, *18* (12), 2789–2795. doi:10.1093/cercor/bhn040

Beppu, K., Sasaki, T., Tanaka, K. F., Yamanaka, A., Fukazawa, Y., Shigemoto, R., & Matsui, K. (2014). Optogenetic countering of glial acidosis suppresses glial glutamate release and ischemic brain damage. *Neuron*, *81* (2), 314–320. doi:10.1016/j.neuron.2013.11.011

Berndt, A., Yizhar, O., Gunaydin, L. A., Hegemann, P., & Deisseroth, K. (2009). Bi-stable neural state switches. *Nature Neuroscience*, *12* (2), 229–234. doi:10.1038/nn.2247

Ekstrom, A. (2010). How and when the fMRI BOLD signal relates to underlying neural activity: The danger in dissociation. *Brain Research Reviews*, *62* (2), 233–244. doi:10.1016/j.brainresrev.2009.12.004

Figley, C. R., & Stroman, P. W. (2011). The role(s) of astrocytes and astrocyte activity in neurometabolism, neurovascular coupling, and the production of functional neuroimaging signals. *The European Journal of Neuroscience*, *33* (4), 577–588. doi:10.1111/j.1460-9568.2010.07584.x

Figueiredo, M., Lane, S., Stout, R. F., Liu, B., Parpura, V., Teschemacher, A. G., & Kasparov, S. (2014). Comparative analysis of optogenetic actuators in cultured

442 astrocytes. *Cell Calcium*, *56* (3), 208–214. doi:10.1016/j.ceca.2014.07.007
443 Gourine, A. V., Kasymov, V., Marina, N., Tang, F., Figueiredo, M. F., Lane, S., …
444 Kasparov, S. (2010). Astrocytes Control Breathing Through pH-Dependent
445 Release of ATP. *Science*, *329* (5991), 571–575. doi:10.1126/science.1190721
446 Greenberg, D. S., Houweling, A. R., & Kerr, J. N. D. (2008). Population imaging of
447 ongoing neuronal activity in the visual cortex of awake rats. *Nature Neuroscience*,
448 *11* (7), 749–751. doi:10.1038/nn.2140
449 Gurden, H. (2013). Astrocytes: can they be the missing stars linking neuronal activity to
450 neurofunctional imaging signals? *Frontiers in Cellular Neuroscience*, *7*.
451 doi:10.3389/fncel.2013.00021
452 Haydon, P. G., & Carmignoto, G. (2006). Astrocyte Control of Synaptic Transmission
453 and Neurovascular Coupling. *Physiological Reviews*, *86* (3), 1009–1031.
454 doi:10.1152/physrev.00049.2005
455 Heeger, D. J., & Ress, D. (2002). What does fMRI tell us about neuronal activity? *Nature*
456 *Reviews. Neuroscience*, *3* (2), 142–151. doi:10.1038/nrn730
457 Jego, P., Pacheco-Torres, J., Araque, A., & Canals, S. (2014). Functional MRI in mice
458 lacking IP3-dependent calcium signaling in astrocytes. *Journal of Cerebral Blood*
459 *Flow and Metabolism*, *34* (10), 1599–1603. doi:10.1038/jcbfm.2014.144
460 Kahn, I., Knoblich, U., Desai, M., Bernstein, J., Graybiel, A. M., Boyden, E. S., … Moore,
461 C. I. (2013). Optogenetic drive of neocortical pyramidal neurons generates fMRI
462 signals that are correlated with spiking activity. *Brain Research*, *1511*, 33–45.
463 doi:10.1016/j.brainres.2013.03.011
464 Lee, J. H., Durand, R., Gradinaru, V., Zhang, F., Goshen, I., Kim, D.-S., … Deisseroth, K.

(2010). Global and local fMRI signals driven by neurons defined optogenetically by type and wiring. *Nature*, *465* (7299), 788–792. doi:10.1038/nature09108

Logothetis, N. K., Pauls, J., Augath, M., Trinath, T., & Oeltermann, A. (2001). Neurophysiological investigation of the basis of the fMRI signal. *Nature*, *412* (6843), 150–157. doi:10.1038/35084005

MacVicar, B. A., Crichton, S. A., Burnard, D. M., & Tse, F. W. (1987). Membrane conductance oscillations in astrocytes induced by phorbol ester. *Nature*, *329* (6136), 242–243. doi:10.1038/329242a0

Maier, A., Wilke, M., Aura, C., Zhu, C., Ye, F. Q., & Leopold, D. A. (2008). Divergence of fMRI and neural signals in V1 during perceptual suppression in the awake monkey. *Nature Neuroscience*, *11* (10), 1193–1200. doi:10.1038/nn.2173

Masamoto, K., & Kanno, I. (2012). Anesthesia and the quantitative evaluation of neurovascular coupling. *Journal of Cerebral Blood Flow and Metabolism*, *32* (7), 1233–1247. doi:10.1038/jcbfm.2012.50

Masamoto, K., Unekawa, M., Watanabe, T., Toriumi, H., Takuwa, H., Kawaguchi, H., … Suzuki, N. (2015). Unveiling astrocytic control of cerebral blood flow with optogenetics. *Scientific Reports*, *5*, 11455. doi:10.1038/srep11455

Mattis, J., Tye, K. M., Ferenczi, E. A., Ramakrishnan, C., O'Shea, D. J., Prakash, R., … Deisseroth, K. (2012). Principles for applying optogenetic tools derived from direct comparative analysis of microbial opsins. *Nature Methods*, *9* (2), 159–172. doi:10.1038/nmeth.1808

Mishra, A., Reynolds, J. P., Chen, Y., Gourine, A. V., Rusakov, D. A., & Attwell, D. (2016). Astrocytes mediate neurovascular signaling to capillary pericytes but not

to arterioles. *Nature Neuroscience*, *19* (12), 1619–1627. doi:10.1038/nn.4428

Morikawa, T., Kajimura, M., Nakamura, T., Hishiki, T., Nakanishi, T., Yukutake, Y., … Suematsu, M. (2012). Hypoxic regulation of the cerebral microcirculation is mediated by a carbon monoxide-sensitive hydrogen sulfide pathway. *Proceedings of the National Academy of Sciences*, *109* (4), 1293–1298. doi:10.1073/pnas.1119658109

Nagaoka, T., Zhao, F., Wang, P., Harel, N., Kennan, R. P., Ogawa, S., & Kim, S.-G. (2006). Increases in oxygen consumption without cerebral blood volume change during visual stimulation under hypotension condition. *Journal of Cerebral Blood Flow and Metabolism*, *26* (8), 1043–1051. doi:10.1038/sj.jcbfm.9600251

Niessing, J., Ebisch, B., Schmidt, K. E., Niessing, M., Singer, W., & Galuske, R. A. W. (2005). Hemodynamic signals correlate tightly with synchronized gamma oscillations. *Science (New York, N.Y.)*, *309* (5736), 948–951. doi:10.1126/science.1110948

Ogawa, S., Lee, T. M., Kay, A. R., & Tank, D. W. (1990). Brain magnetic resonance imaging with contrast dependent on blood oxygenation. *Proceedings of the National Academy of Sciences of the United States of America*, *87* (24), 9868–9872.

Ogawa, S., Menon, R. S., Kim, S. G., & Ugurbil, K. (1998). On the characteristics of functional magnetic resonance imaging of the brain. *Annual Review of Biophysics and Biomolecular Structure*, *27*, 447–474. doi:10.1146/annurev.biophys.27.1.447

Otsu, Y., Couchman, K., Lyons, D. G., Collot, M., Agarwal, A., Mallet, J.-M., … Charpak, S. (2015). Calcium dynamics in astrocyte processes during neurovascular

511 coupling. *Nature Neuroscience*, *18* (2), 210–218. doi:10.1038/nn.3906
512 Pankratov, Y., & Lalo, U. (2015). Role for astroglial α1-adrenoreceptors in
513 gliotransmission and control of synaptic plasticity in the neocortex. *Frontiers in*
514 *Cellular Neuroscience*, *9*, 230. doi:10.3389/fncel.2015.00230
515 Pelluru, D., Konadhode, R. R., Bhat, N. R., & Shiromani, P. J. (2016). Optogenetic
516 stimulation of astrocytes in the posterior hypothalamus increases sleep at night in
517 C57BL/6J mice. *The European Journal of Neuroscience*, *43* (10), 1298–1306.
518 doi:10.1111/ejn.13074
519 Perea, G., Yang, A., Boyden, E. S., & Sur, M. (2014). Optogenetic astrocyte activation
520 modulates response selectivity of visual cortex neurons in vivo. *Nature*
521 *Communications*, *5*. doi:10.1038/ncomms4262
522 Pettegrew, J. W., Levine, J., & McClure, R. J. (2000). Acetyl-L-carnitine
523 physical-chemical, metabolic, and therapeutic properties: relevance for its mode
524 of action in Alzheimer's disease and geriatric depression. *Molecular Psychiatry*, *5*
525 (6), 616–632.
526 Petzold, G. C., & Murthy, V. N. (2011). Role of Astrocytes in Neurovascular Coupling.
527 *Neuron*, *71* (5), 782–797. doi:10.1016/j.neuron.2011.08.009
528 Raichle, M. E., & Mintun, M. A. (2006). Brain work and brain imaging. *Annual Review of*
529 *Neuroscience*, *29*, 449–476. doi:10.1146/annurev.neuro.29.051605.112819
530 Rose, C. R., & Ransom, B. R. (1996). Mechanisms of H+ and Na+ Changes Induced by
531 Glutamate, Kainate, and d-Aspartate in Rat Hippocampal Astrocytes. *The Journal*
532 *of Neuroscience*, *16* (17), 5393–5404.
533 Sasaki, T., Beppu, K., Tanaka, K. F., Fukazawa, Y., Shigemoto, R., & Matsui, K. (2012).

534 Application of an optogenetic byway for perturbing neuronal activity via glial
535 photostimulation. *Proceedings of the National Academy of Sciences of the United*
536 *States of America*, *109* (50), 20720–20725. doi:10.1073/pnas.1213458109
537 Schulz, K., Sydekum, E., Krueppel, R., Engelbrecht, C. J., Schlegel, F., Schröter, A., …
538 Helmchen, F. (2012). Simultaneous BOLD fMRI and fiber-optic calcium
539 recording in rat neocortex. *Nature Methods*, *9* (6), 597–602.
540 doi:10.1038/nmeth.2013
541 Schummers, J., Yu, H., & Sur, M. (2008). Tuned Responses of Astrocytes and Their
542 Influence on Hemodynamic Signals in the Visual Cortex. *Science*, *320* (5883),
543 1638–1643. doi:10.1126/science.1156120
544 Seigneur, J., Kroeger, D., Nita, D. A., & Amzica, F. (2006). Cholinergic Action on
545 Cortical Glial Cells In Vivo. *Cereb. Cortex*, *16* (5), 655–668.
546 doi:10.1093/cercor/bhj011
547 Sekiguchi, K. J., Shekhtmeyster, P., Merten, K., Arena, A., Cook, D., Hoffman, E., …
548 Nimmerjahn, A. (2016). Imaging large-scale cellular activity in spinal cord of
549 freely behaving mice. *Nature Communications*, *7*, 11450.
550 doi:10.1038/ncomms11450
551 Shen, Q., Ren, H., & Duong, T. Q. (2008). CBF, BOLD, CBV, and CMRO2 fMRI Signal
552 Temporal Dynamics at 500-msec Resolution. *Journal of Magnetic Resonance*
553 *Imaging : JMRI*, *27* (3), 599–606. doi:10.1002/jmri.21203
554 Sirotin, Y. B., & Das, A. (2009). Anticipatory haemodynamic signals in sensory cortex
555 not predicted by local neuronal activity. *Nature*, *457* (7228), 475–479.
556 doi:10.1038/nature07664

Sokoloff, L., Reivich, M., Kennedy, C., Rosiers, M. H. D., Patlak, C. S., Pettigrew, K. D., … Shinohara, M. (1977). The [14C]deoxyglucose Method for the Measurement of Local Cerebral Glucose Utilization: Theory, Procedure, and Normal Values in the Conscious and Anesthetized Albino Rat. *Journal of Neurochemistry*, *28* (5), 897–916. doi:10.1111/j.1471-4159.1977.tb10649.x

Srinivasan, R., Huang, B. S., Venugopal, S., Johnston, A. D., Chai, H., Zeng, H., … Khakh, B. S. (2015). Ca2+ signaling in astrocytes from Ip3r2-/- mice in brain slices and during startle responses in vivo. *Nature Neuroscience*, *18* (5), 708–717. doi:10.1038/nn.4001

Stark, J. A., Davies, K. E., Williams, S. R., & Luckman, S. M. (2006). Functional magnetic resonance imaging and c-Fos mapping in rats following an anorectic dose of m-chlorophenylpiperazine. *NeuroImage*, *31* (3), 1228–1237. doi:10.1016/j.neuroimage.2006.01.046

Stobart, J. L., Ferrari, K. D., Barrett, M. J. P., Stobart, M. J., Looser, Z. J., Saab, A. S., & Weber, B. (2016). Long-term In Vivo Calcium Imaging of Astrocytes Reveals Distinct Cellular Compartment Responses to Sensory Stimulation. *Cerebral Cortex*. doi:10.1093/cercor/bhw366

Sugiura, Y., Honda, K., Kajimura, M., & Suematsu, M. (2014). Visualization and quantification of cerebral metabolic fluxes of glucose in awake mice. *Proteomics*, *14* (7–8), 829–838. doi:10.1002/pmic.201300047

Sugiura, Y., Honda, K., & Suematsu, M. (2015). Development of an Imaging Mass Spectrometry Technique for Visualizing Localized Cellular Signaling Mediators in Tissues. *Mass Spectrometry*, *4* (1), 1–9. doi:10.5702/massspectrometry.A0040

580 Sugiura, Y., Katsumata, Y., Sano, M., Honda, K., Kajimura, M., Fukuda, K., & Suematsu,
581 M. (2016). Visualization of in vivo metabolic flows reveals accelerated utilization
582 of glucose and lactate in penumbra of ischemic heart. *Scientific Reports*, *6*, 32361.
583 doi:10.1038/srep32361
584 Sugiura, Y., Taguchi, R., & Setou, M. (2011). Visualization of spatiotemporal energy
585 dynamics of hippocampal neurons by mass spectrometry during a
586 kainate-induced seizure. *PloS One*, *6* (3), e17952.
587 doi:10.1371/journal.pone.0017952
588 Takano, T., Tian, G.-F., Peng, W., Lou, N., Libionka, W., Han, X., & Nedergaard, M.
589 (2006). Astrocyte-mediated control of cerebral blood flow. *Nat Neurosci*, *9* (2),
590 260–267. doi:10.1038/nn1623
591 Takata, N., Mishima, T., Hisatsune, C., Nagai, T., Ebisui, E., Mikoshiba, K., & Hirase, H.
592 (2011). Astrocyte calcium signaling transforms cholinergic modulation to cortical
593 plasticity in vivo. *The Journal of Neuroscience*, *31* (49), 18155–18165.
594 doi:10.1523/JNEUROSCI.5289-11.2011
595 Takata, N., Yoshida, K., Komaki, Y., Xu, M., Sakai, Y., Hikishima, K., … Tanaka, K. F.
596 (2015). Optogenetic activation of CA1 pyramidal neurons at the dorsal and
597 ventral hippocampus evokes distinct brain-wide responses revealed by mouse
598 fMRI. *PloS One*, *10* (3), e0121417. doi:10.1371/journal.pone.0121417
599 Tanaka, K. F., Matsui, K., Sasaki, T., Sano, H., Sugio, S., Fan, K., … Yamanaka, A.
600 (2012). Expanding the repertoire of optogenetically targeted cells with an
601 enhanced gene expression system. *Cell Reports*, *2* (2), 397–406.
602 doi:10.1016/j.celrep.2012.06.011

603 Tang, F., Lane, S., Korsak, A., Paton, J. F. R., Gourine, A. V., Kasparov, S., &
604 Teschemacher, A. G. (2014). Lactate-mediated glia-neuronal signalling in the
605 mammalian brain. *Nature Communications*, *5*, 3284. doi:10.1038/ncomms4284
606 Thrane, A. S., Thrane, V. R., Zeppenfeld, D., Lou, N., Xu, Q., Nagelhus, E. A., &
607 Nedergaard, M. (2012). General anesthesia selectively disrupts astrocyte calcium
608 signaling in the awake mouse cortex. *Proceedings of the National Academy of*
609 *Sciences of the United States of America*, *109* (46), 18974–18979.
610 doi:10.1073/pnas.1209448109
611 Traina, G. (2016). The neurobiology of acetyl-L-carnitine. *Frontiers in Bioscience*
612 *(Landmark Edition)*, *21*, 1314–1329.
613 Tsurugizawa, T., Ciobanu, L., & Le Bihan, D. (2013). Water diffusion in brain cortex
614 closely tracks underlying neuronal activity. *Proceedings of the National Academy*
615 *of Sciences of the United States of America*. doi:10.1073/pnas.1303178110
616 Vanzetta, I., & Slovin, H. (2010). A BOLD Assumption. *Frontiers in Neuroenergetics*, *2*.
617 doi:10.3389/fnene.2010.00024
618 Yoshida, K., Mimura, Y., Ishihara, R., Nishida, H., Komaki, Y., Minakuchi, T., … Takata,
619 N. (2016). Physiological effects of a habituation procedure for functional MRI in
620 awake mice using a cryogenic radiofrequency probe. *Journal of Neuroscience*
621 *Methods*, *274*, 38–48. doi:10.1016/j.jneumeth.2016.09.013

Figure Legends

Figure 1. Transgenic mice that express ChR2(C128S)-EYFP at neurons or astrocytes.

(**a, d**) Immunostaining against YFP (ChR2-marker) on coronal sections of the brain from Neuron- (**a**) and Astrocyte-ChR2 mice (**d**). (**b, e**) Double-immunostaining for NeuN (neuron marker, red) and YFP (green) of coronal sections of the brain from Neuron- (**b**) and Astrocyte-ChR2 mice (**e**). (**c, f**) Higher magnification images of cortical layer IV of Neuron- or Astrocyte-ChR2 mice. (**g**) Schematic drawings of attachment of a headbar (gray) and an optic fiber with a cannula (red) on the intact skull. A headbar was used for cranial fixation during ofMRI in awake mice. (**h**) A photograph of a transgenic mouse with an attached headbar (arrow head) and a fiber optic cannula (arrow). (**i**) Estimated area of illumination (pale blue) by an optic fiber (red), drawn over a horizontal (left) and a sagittal (right) brain section of an anatomical MRI image. Scale bar: **a,d,** 3 mm; **b,e,** 200 μm; **c,f,** 50 μm; **g,h,i,** 5 mm.

Figure 2. Transcranial optogenetic stimulation of neurons or astrocytes evoked BOLD signal response with oxygen consumption.

(**a, c**) Activation *t*-maps overlaid on structural MRI images showing spatial distribution of positive BOLD response upon optogenetic activation of cortical neurons (**a**) or astrocytes (**c**) from n = 13 Neuron- or 9 Astrocyte-ChR2 mice, respectively. Illumination was applied on the left side of the skull (left side in the figure). Values at the lower left indicate anterior-posterior (AP) distance from bregma in mm. Color bar indicates *t*-values. Arrows at AP -4.0 and -3.0 mm in (**a**) and (**c**), respectively, indicate approximate position of a global peak of *t*-values, which were used for locations of ROIs for BOLD time

courses. (**b, d**) Time-course of BOLD signal fluctuation upon optogenetic activation of neurons (**b**) or astrocytes (**d**). Blue and yellow vertical lines show timing of illumination for each color. Note that ChR2(C128S), a step function opsin with the closing time constant (τ) of 106 s, was kept open even after cessation of blue illumination until yellow illumination. The x-axis at the top shows the scan number of fMRI measurements. Gray shading indicates the SEM. (**e–h**) The same as (**a–d**), but in the presence of a vasodilator, SNP, from n = 3 Neuron- or 3 Astrocyte-ChR2 mice, respectively, showing negative BOLD response that indicates oxygen consumption upon optogenetic activation of neurons (**f**) or astrocytes (**h**). Scale bar: **a, c, e, g,** 2 mm.

Figure 3. Optogenetic stimulation of neurons, but not astrocytes, results in neuronal activation.

(**a, b**) Representative images of *in situ* hybridization on coronal brain sections around AP -2.0 mm for *c-fos* mRNA, 30 min after optogenetic stimulation of cortical neurons (**a**) or astrocytes (**b**) using Neuron- or Astrocyte-ChR2 mice, respectively (n = 9 each). Optogenetic stimulation of neurons, but not astrocytes, induced expression of *c-fos* mRNA (blue-purple signal) in the cortex ipsilateral to light illumination. Rectangles in blue and red were for quantification of staining intensity of *c-fos* mRNA. Scale bar: 1 mm. (**c, d**) LFP fluctuations upon optogenetic stimulation of Neuron- (**c**) or Astrocyte-ChR2 mice (**d**). **Upper left:** Representative traces of LFP recorded with a silicon probe electrode, inserted into the cortex of an awake Neuron- (**c**) or Astrocyte-ChR2 mouse (**d**). The blue area indicates the period of blue-light illumination. Note that the duration of light illumination was 0.5 and 5.0 s for Neuron- and Astrocyte-ChR2 mice, respectively. **Upper right:** Mean wavelet power spectrogram of LFP recorded in the cortex of n = 6 Neuron- (**c**) or n = 5 Astrocyte-ChR2 mice (**d**). Power values of LFP were normalized for

each recording session (see methods). Blue and yellow triangles with white vertical lines indicate the delivery of blue and yellow light pulses, respectively. **Lower left:** Mean time courses of LFP-power at each frequency band. Vertical lines of blue and yellow indicate the delivery of light pulses of each color. The SEM envelopes the mean traces. **Lower right:** The bar graph compares the mean power of LFP at each frequency band during the first activation period (60~90 s). No modulation of LFP power was observed in Astrocyte-ChR2 mice (**d**). *$P < 0.05$, **$P < 0.01$; paired *t*-test. (**e, f**) MUA response upon optogenetic stimulation of Neuron- (**e**) or Astrocyte-ChR2 mice (**f**). **Upper left:** A representative time course of high-pass filtered LFP (upper trace) and MUA (lower trace). A horizontal red line in the upper trace indicates a threshold for MUA extraction. **Upper right:** Representative mean traces of MUA during a baseline period (0~60 s, blue), and 1st (60~90 s, green), 2nd (210~240 s, red), and 3rd (360~390 s, pale blue) activation periods. **Lower panel:** Relative number of MUA counts, recorded from the most superficial 10 channels of the silicon probe in the cortex, from n = 6 Neuron- (**e**) and n = 5 Astrocyte-ChR2 mice (**f**). The SEM envelopes the mean traces.

Figure 4. Synthesis of AC at the site of optogenetic activation of astrocytes, but not of neurons.

(**a**) **Upper panel:** Schematic of IMS experiments, which involved pathway tracing of $^{13}C_6$-labeled glucose upon optogenetic stimulation. A red circle indicates ^{13}C-isotope in a glucose molecule. Optic fiber was attached on the left intact skull. **Lower panel:** Experimental time course. FMW fixation of the brain was performed 30 s following optogenetic stimulation. (**b**) Schematic representation of $^{13}C_6$-glucose metabolism into acetyl-carnitine (AC). (**c, d**) Representative IMS images for carnitine (right top), AC (left middle), $^{13}C_2$-AC (middle right), AC/carnitine ratio (left bottom), and $^{13}C_2$-AC/carnitine

694 ratio (right bottom), after optogenetic stimulation of a Neuron- (**c**) or an Astrocyte-ChR2
695 mouse (**d**). Astrocyte activation augmented synthesis of AC that accompanies O_2
696 consumption (**d**, left middle). Upper left panel shows optical images of brain sections
697 used for IMS. Each panel shows three consecutive slices. Dotted circles in a top right
698 panel in (**d**) indicates area that showed reduction of carnitine. These experiments were
699 repeated with n = 3 Neuron- and n = 5 Astrocyte-ChR2 mice, obtaining similar results.
700 Scale bar: **c,d,** 2 mm.

Figure 1

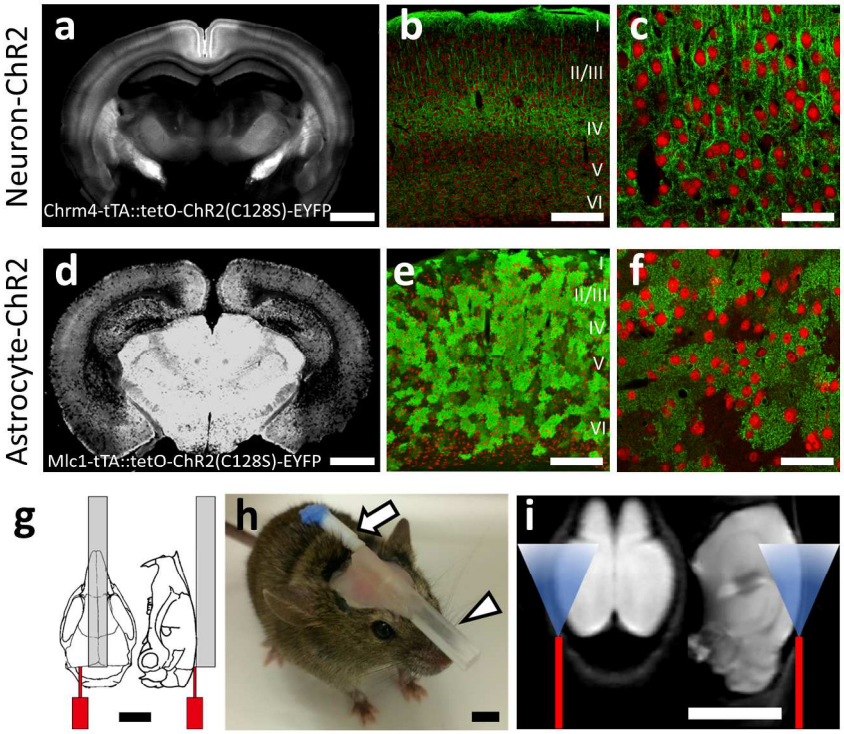

Figure 1. Transgenic mice that express ChR2(C128S)-EYFP at neurons or astrocytes.

190x254mm (300 x 300 DPI)

Figure 2

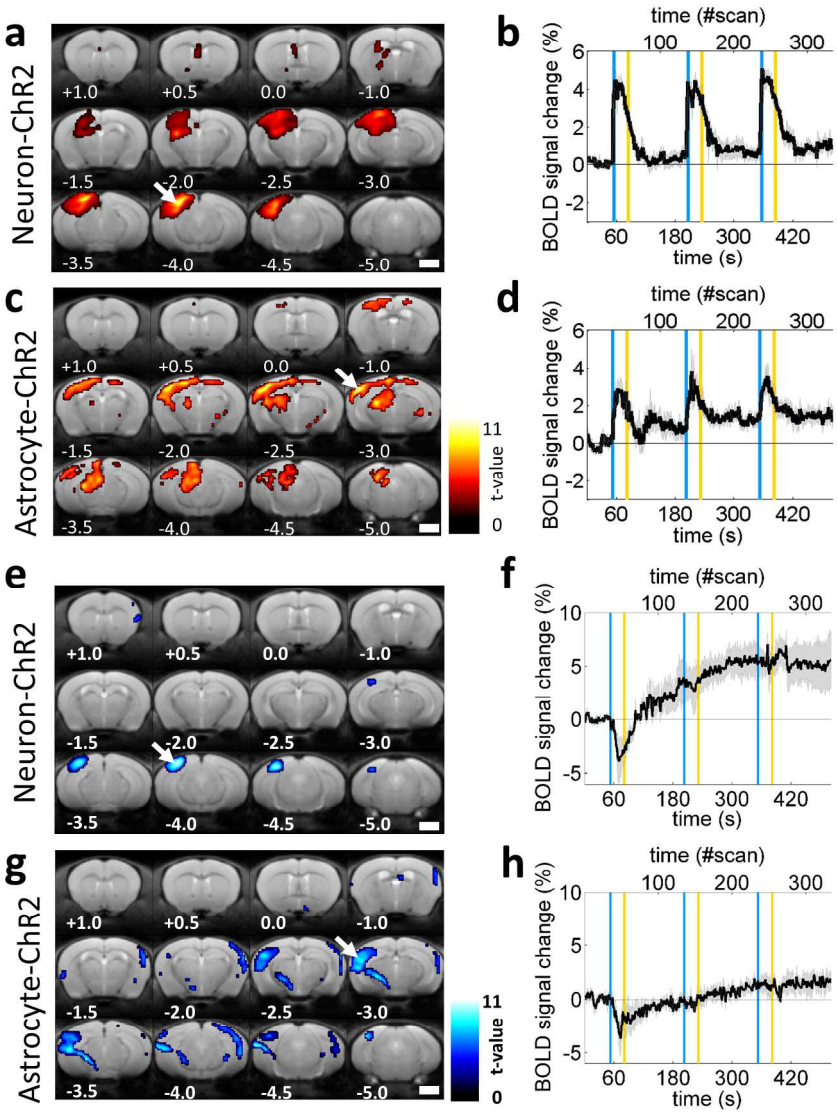

Figure 2. Transcranial optogenetic stimulation of neurons or astrocytes evoked BOLD signal response with oxygen consumption.

190x254mm (300 x 300 DPI)

Figure 3

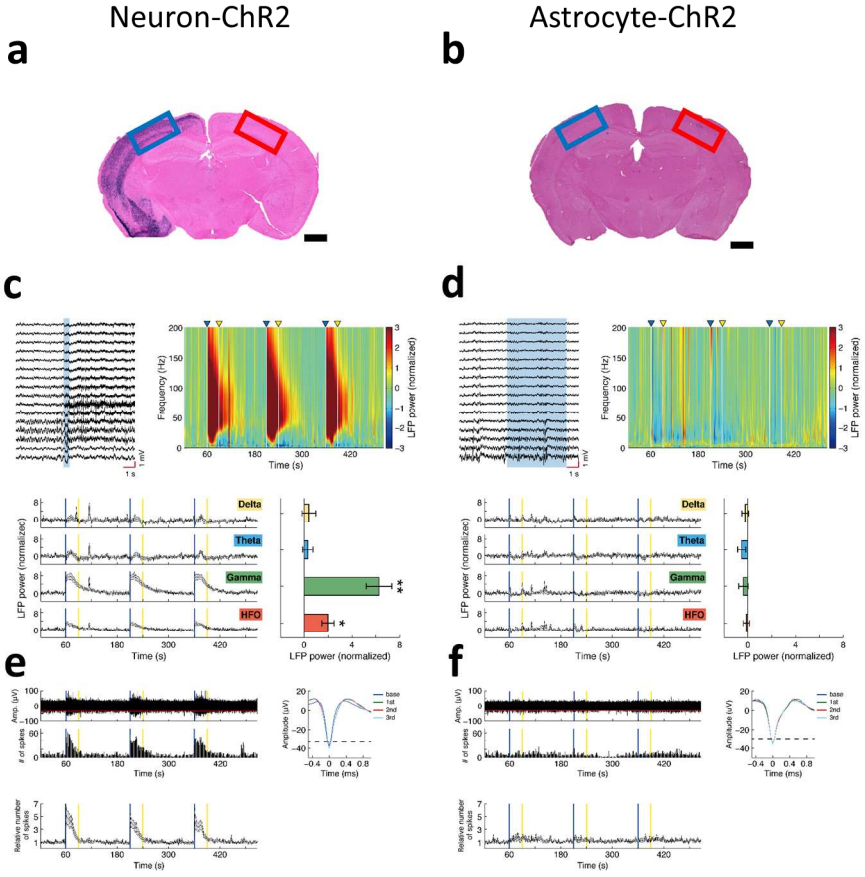

Figure 3. Optogenetic stimulation of neurons, but not astrocytes, results in neuronal activation.

190x254mm (300 x 300 DPI)

Figure 4

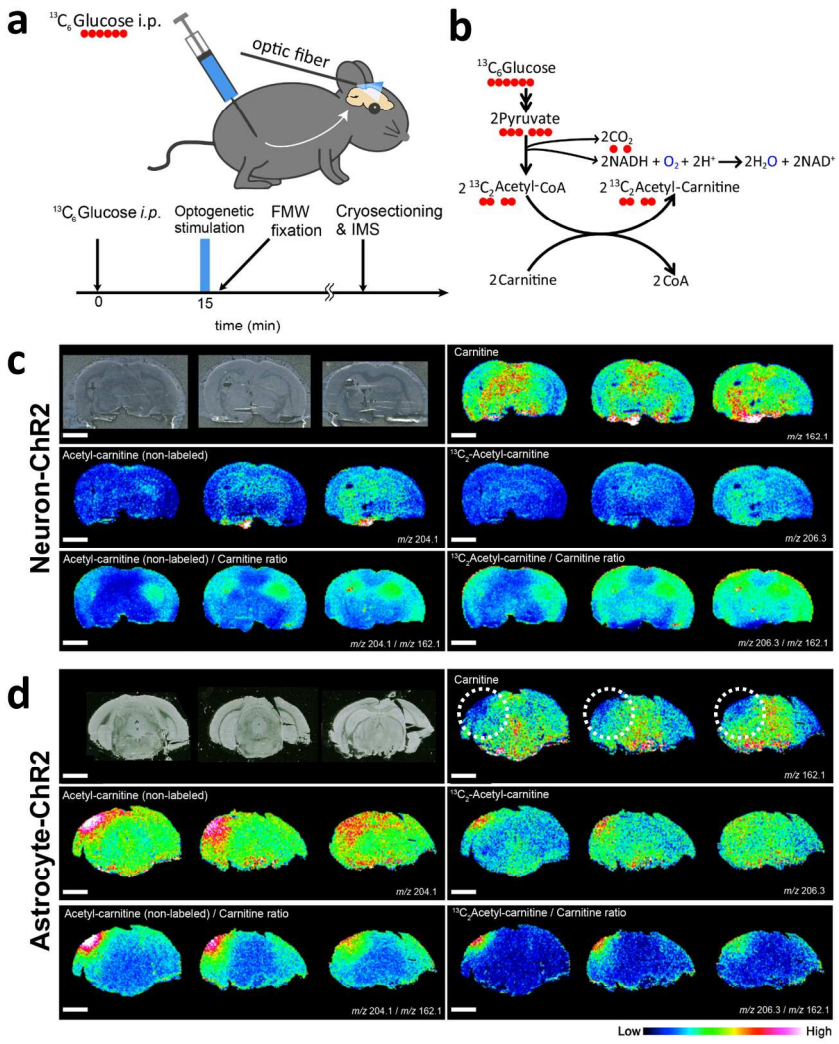

Figure 4. Synthesis of AC at the site of optogenetic activation of astrocytes, but not of neurons.

190x254mm (300 x 300 DPI)

Running title: Astrocytes evoke BOLD fMRI response

Supplementary Materials and Methods

Ethics Statement

All animal experiments were conducted in accordance with the National Institutes of Health Guide for Care and Use of Laboratory Animals (NIH Publications No. 8023) and approved by the Animal Ethics Committee of Keio University (approval number: 12034-(3)) and CIEA (16062A).

Generation of Chrm4-tTA BAC transgenic mice

Mouse BAC DNA (clone RP23-138P5) was modified by inserting a codon optimized tTA (mtTA)-SV40 pA cassette (Tanaka et al., 2010) into the translation initiation site of *Chrm4* gene. Modified BAC DNA was linearized by PI-SceI enzyme digestion (New England Biolabs Inc., Ipswich, MA, USA), and injected into fertilized eggs from CBA/C57BL6 mice. For genotyping of *Chrm4*-tTA line, the following primer set Chrm-394U (5'-AAGCACCAAGTTCTCTCCCGTCTT-3') and mtTAL24 (5'-cggagttgatcaccttggacttgt-3') was used and the transgenic line yielded 430 bp product.

Generation of ChR2(C128S) expressing lines

Double transgenic mice of *Chrm4*-tTA::tetO-ChR2(C128S)-EYFP and *Mlc1*-tTA::tetO-ChR2(C128S)-EYFP were prepared for experiments. *Mlc1*-tTA BAC transgenic mouse (RIKEN BRC stock number:05450) and tetO-ChR2(C128S)-EYFP knockin mouse (RIKEN BRC stock number: 05454) were obtained from RIKEN BioResource Center, JAPAN, and the methods for genotyping were previously described (Kanemaru et al., 2014; Tanaka et al., 2012).

Surgery for attaching an optical fiber and a head-holder on the skull of the mice

In total, 51 double transgenic mice, postnatal 8–12 weeks old, were used; 26 were *Chrm4*-tTA::tetO-ChR2(C128S) mice (9 males and 17 females) and 25 were *Mlc1*-tTA::tetO-ChR2(C128S)-EYFP mice (13 males and 12 females). Animals were anesthetized with a mixture of ketamine and xylazine (100 mg/kg and 10 mg/kg, respectively, i.p.). After skull exposure, an optical fiber of silica glass (Φ 400 μm, CFML14L05, Thorlabs, NJ, USA) was placed on the surface of the skull horizontally to the bregma-lambda line. The side of an optical fiber was painted in black to avoid stray light. The tip of an optical fiber was located at -5.1 mm posterior to the Bregma (AP -5.1 mm), 3.0 mm lateral from the midline to the left (ML -3.0 mm), and 0.6 mm ventral from the horizontal plane passing through bregma and lambda on the surface of the skull (DV +0.6 mm). The tip of an optical fiber was imbedded with a transparent silicone (Φ 200 μm, Kwik-Sil Adhesive, WPI, FL, USA). Optical fiber was then attached on the skull with dental acrylic (Super-Bond C&B, Sun Medical, Shiga, Japan). In the case of IMS experiments, an optical fiber of plastic (Φ 500 μm, Eska SK20, Mitsubishi Chemical, Tokyo, Japan) was used instead of an optical fiber of silica glass.

Next, a custom-made acrylic head bar ($3 \times 3 \times 27$ mm^3) was mounted along the sagittal suture of the exposed skull using the dental cement for fMRI in awake mice (Yoshida et al., 2016). For experiments of *in vivo* electrophysiology, a custom-made U-shaped plastic plate was attached on the skull instead of a head bar to enable fixation of the mouse's head to a stereotaxic frame (SR-6M-HT, Narishige, Tokyo, Japan) during recording. For IMS experiments, a head-holder was not attached because a head of a

mouse is fixed in a dedicated tube (WJM-24 or WJM-28, Muromachi Kikai, Tokyo, Japan). After covering the exposed skull with the dental acrylic, the animal was returned to its homecage for recovery (Yoshida et al., 2016).

fMRI in awake mice

Mice were acclimated to mock fMRI environment for 2 hrs/day for at least 7 days before performing fMRI in awake mice (Yoshida et al., 2016). Structural and functional MRI was performed as described previously (Komaki et al., 2016; Takata et al., 2015) using a 7.0-Tesla MRI apparatus equipped with actively shielded gradients at a maximum strength of 700 mT/m (Biospec 70/16, Bruker BioSpin AG, Fällanden, Switzerland) with a cryogenically cooled 2-ch transmit/receive phased array surface coil (CryoProbe, Z120046, Bruker BioSpin AG, Fällanden, Switzerland), and the ParaVision 5.1 software interface (Bruker Biospin AG, Fällanden, Switzerland). Structural T2-weighted images were acquired using a rapid acquisition process with a relaxation enhancement (RARE) sequence in coronal orientations (repetition time [TR], 6100 ms; echo time [TE], 48 ms; spectral bandwidth [BW], 5 kHz; RARE factor, 8; number of averages, 4; number of slices 52; spatial resolution, $75 \times 75 \times 300$ μm^3). Before fMRI measurement, a field map was acquired to reduce signal loss artifacts (TE, 1.520 ms; 5.325 ms; TR, 20 ms; spatial resolution, $300 \times 300 \times 300$ μm^3; matrix, $64 \times 64 \times 64$ voxels). fMRI was performed using a gradient-echo echo-planar sequence (TR, 1500 ms; TE, 20 ms; BW, 250 kHz; flip angle, 50°; number of segments, 1; number of averages 1; number of slices 18; spatial resolution, $200 \times 200 \times 500$ μm^3; FOV, 19.2×19.2 mm^2; matrix, $96 \times 96 \times 18$ voxels). This functional image covered the whole brain except the olfactory bulb and the cerebellum. Total scanning time was 8.5 min (340 volumes with a

1.5-s interval). In ofMRI experiments in the presence of a nitric oxide donor, subcutaneous injection of S-nitroprusside (SNP, 10 mg/kg, Sigma-Aldrich, MO, USA) was performed five minutes before the start of fMRI measurements (Nagaoka et al., 2006; Tsurugizawa, Ciobanu, & Le Bihan, 2013; Yamamoto, 1992).

Transcranial light illumination

A pair of blue and yellow light pulses with 30-s intervals (1.1~2.5 mW at the tip of an optical fiber; LEDC2-B/A, Doric Lenses, QC, Canada) were delivered 60-s after the start of fMRI measurements. Pulse duration was 0.5 s and 5 s for experiments with Neuron- and Astrocyte-ChR2 mice, respectively. In the case of IMS experiments, only the first blue light was delivered, 30–40 s after which FMW was applied to inactivate enzymatic reactions in the brain. Area of illumination was estimated to cover the left parietal cortex based on calculation using numerical aperture and diameter of the optic fiber without considering light scattering in the skull and the cerebral parenchyma (Fig. 1i). Power of illuminated light beneath the skull was estimated to be ~5% of that at the tip of an optical fiber, based on our measurement using a power meter (PM160T, Thorlabs, NJ, USA; detector ø10 mm) that was put beneath the skull (0.15 and 2.7 mW, respectively). Estimated irradiance beneath the skull is ~0.002 mW/mm^2, which corresponds to half-maximal activation (EPD50) of ChR2(C128S) (Mattis et al., 2012).

In vivo multichannel extracellular recordings

Extracellular recording was made from awake transgenic mice using a 16-channel, linear silicon probe (100-μm spacing, 177-μm^2 recording site area; NeuroNexus, MI, USA), which was inserted through a craniotomy (Φ 0.5 mm; AP -3.0 mm, ML -2.0 mm) at a depth of 1.7 mm ventrally from the pia for recording from the

cortex. The craniotomy was sealed with a mixture of wax and paraffin oil. Recording sessions started > 1 h after insertion of the silicon probe for recovery (Takata et al., 2014). Electrophysiological signals were recorded with a RZ2 neurophysiology workstation (Tucker-Davis Technologies, FL, USA).

IMS with FMW-assisted brain fixation for $^{13}C_6$-glucose metabolic pathway tracing

To trace the metabolic fate of glucose, $^{13}C_6$-glucose (1 mg/g body weight, in saline) was injected intraperitoneally. Fifteen minutes later (Sugiura, Honda, Kajimura, & Suematsu, 2014), optogenetic stimulation of neurons or astrocytes was performed with illumination of blue light for 0.5 or 5 s transcranially on the left hemisphere of the brain of Neuron- or Astrocyte-ChR2 mice, respectively. Mice were then confined in a tubulous, water-jacket holder (WJM-24 or 28, Muromachi Kikai, Tokyo, Japan), and placed inside a microwave fixation system (MMW-05, Muromachi Kikai, Tokyo, Japan). Thirty seconds after the optogenetic stimulation, mice were euthanized by FMW-irradiation on the brain (5 kW for 0.96 s), which immediately elevated the temperature of the brain up to 80°C to inactivate metabolic enzymes and minimize postmortem changes in labile metabolites (Sugiura, Honda, & Suematsu, 2015). After microwave irradiation, brains were dissected with a surgical knife at room temperature, embedded into a super cryo-embedding medium (SCEM, Section Lab, Hiroshima, Japan), rapidly frozen in liquid N_2, and stored at -80°C.

Thin sections of the frozen brain were prepared with a cryomicrotome (CM3050, Leica Microsystems, Wetzlar, Germany) and thaw-mounted on an indium thin oxide-coated glass slide (Bruker Daltonics, Leipzig, Germany) at -16°C. Slices were then

manually spray-coated with 9-aminoacridine (10 mg/mL, dissolved in 80% ethanol) and 2,5-dihydroxybenzoic acid (DHB) as a matrix (50 mg/mL, dissolved in 80% ethanol) for anion and cation metabolites, respectively. Matrix-assisted laser desorption ionization (MALDI)-IMS was performed using an Ultra Flextreme MALDI-TOF mass spectrometer (Bruker Daltonics, Leipzig, Germany) equipped with an Nd:YAG laser. The laser power was optimized to minimize in-source decay of phosphate of nucleotides. Data were acquired in the reflectron mode with raster scanning using a pitch distance of 100 μm. Each mass spectrum was the result of 300 laser shots at each data point. Signals between *m/z* 50 and 1000 were collected. Molecular identification was performed based on previous reports (Sugiura et al., 2014; Sugiura, Taguchi, & Setou, 2011). Image reconstruction was performed using FlexImaging 4.0 software (Bruker Daltonics, Leipzig, Germany).

Histology

After measurements, animals were deeply anesthetized and transcardially perfused with PB containing 4% PFA. Immunohistochemistry of EYFP to confirm neuronal or astrocytic expression of ChR2(C128S)-EYFP was performed using affinity-purified antibodies against heat-denatured GFP (a gift from Dr. Kouichi C. Nakamura) (Nakamura, Kameda, Koshimizu, Yanagawa, & Kaneko, 2008). *In situ* hybridization to examine *c-fos* mRNA expression was performed as reported previously (Takata et al., 2015).

Data processing and analysis

Analysis of fMRI data was performed using SPM12 software (www.fil.ion.ucl.ac.uk/spm) as previously (Takata et al., 2015; Yoshida et al.,

2016). This consisted of head movement correction, adjustments of acquisition timing across slices, and smoothing using a Gaussian kernel of 0.4-mm full width at half maximum. Structural and functional images were spatially normalized to a standard structural brain averaged from 20 C57BL/6 mice. Statistical *t*-maps were calculated using a generalized linear model (GLM) with random effects using a block design regarding the optogenetic activation, delayed vascular response and head movement. Activation was detected using a statistical threshold of uncorrected $P < 0.005$ and a cluster size > 10, which were objectively chosen via Monte Carlo simulations using the "AlphaSim" implementation in a toolbox REST (Song et al., 2011), resulting in a family-wise error rate of $P < 0.05$. The parameters used for the simulations were as follows: full width at half maximum, 0.4 mm; cluster connection radius, 0.2 mm; individual voxel threshold probability, 0.005; number of Monte Carlo iterations, 100,000; voxels in mask, 13441. Timecourses of BOLD signals were obtained with a spherical ROI of 0.7-mm diameter, using the SPM toolbox MarsBar (http://marsbar.sourceforge.net).

Electrophysiological data analysis was performed using MATLAB (R2014a, MathWorks, MA, USA). LFPs were decomposed to frequency bands of delta (1–4 Hz), theta (6–9 Hz), gamma (40–90 Hz), and high frequency oscillation (HFO; 140–200 Hz) (Buzsáki et al., 2003). Power values of LFP were logged and z-scored by each frequency band with its mean and standard deviation (SD) during the period before the first blue illumination for each recording session (Carr, Karlsson, & Frank, 2012). MUA was extracted by thresholding the high-pass filtered LFP (> 300 Hz) with 4σ where σ = median{absolute value of the filtered LFP / 0.6745} (Quiroga, Nadasdy, & Ben-Shaul, 2004). Count of MUA was binned to 1.5 s. Data are expressed as mean ±

SEM across animals, except where otherwise noted. Two-tailed *t*-tests were used for comparisons of two population means, unless otherwise noted.

Supplementary Results

Optogenetic stimulation of astrocytes as well as neurons evokes BOLD signal response.

Subcortical BOLD signal in Astrocyte-ChR2 mice may reflect direct photo-activation of astrocytes

Other than the cortex, a BOLD signal response was observed in the hippocampus and thalamus of Neuron- and Astrocyte-ChR2 mice, respectively (Fig. 2a, c). Subcortical BOLD signal in Astrocyte-ChR2 mice may reflect direct photo-activation of astrocytes due to an especially high expression level of ChR2(C128S) (Fig. 1d), and higher sensitivity of ChR2(C128S), which is ~1000 times more sensitive than conventional ChR2 (Mattis et al., 2012). To confirm this scenario, we generated a triple transgenic mice (Astrocyte-ChR2 mice with *Emx1*-Cre) that express ChR2(C128S) in astrocytes of ventral but not dorsal part of the brain (Supplementary Fig. 2a, b). Transcranial illumination of Astrocyte-ChR2 mice with *Emx1*-Cre evoked BOLD signal response in subcortical region, indicating that sufficient amount of light reached the subcortical region to activate ChR2(C128S) (Supplementary Fig. 2c, d).

Light illumination for optogenetic stimulation seemed not enough to evoke BOLD signal response through visual stimulation nor brain-tissue heating

Illumination using only yellow light, which does not open ChR2(C128S), did not evoke BOLD signal fluctuations in neither Neuron- nor Astrocyte-ChR2 mice

(Supplementary Fig. 3a, b). This suggests that the BOLD signal response was not derived from activation of the visual pathways of mice (Schmid et al., 2016); nor was it an artefact of the illumination heating the brain tissue (Christie et al., 2012). It is recently shown that blue light triggers arteriole dilations, independently of heat (Rungta, Osmanski, Boido, Tanter, & Charpak, 2017). Amount of light used in our study (0.15 mW for 0.5 or 5 s; see Supplementary Materials and Methods) is below the lower limit of the effect (0.5~1 mW for 2 s with 40% duty cycle). Also note that the reported blood flow increases by blue light *per se* returned to baseline shortly, while our BOLD signal response lasted more than 30 s after blue light illumination because ChR2(C128S) is a step-function opsin. Moreover, we reported previously that blue light illumination with higher power (1~2 mW for 0.5 s) did not evoke BOLD signal fluctuation in wild type mice (Takata et al., 2015).

Behavioral state change seemed not to contaminate BOLD signal fluctuation upon optogenetic activation of astrocytes or neurons

It's reported that change in behavioral state of mice (*i.e.* locomotion and startle response) may cause widespread astrocyte excitation in the brain (Nimmerjahn, Mukamel, & Schnitzer, 2009; Paukert et al., 2014; Srinivasan et al., 2015). If optogenetic stimulation results in behavioral response, it's possible that BOLD signal fluctuation in our study may reflect behavioral state-change that results in astrocyte excitation, rather than optogenetic astrocyte activation. To address this possibility, we performed open-field tests using Neuron-ChR2 or Astrocyte-ChR2 mice. Light illumination did not evoke overt motor responses in our experimental condition (Supplementary Fig. 4). Moreover, we performed ofMRI using *anesthetized* Astrocyte-ChR2 mice, demonstrating

BOLD signal response upon optogenetic astrocyte activation (Supplementary Fig. 2e, f). These results imply that behavioral state-change was not a dominant cause for the BOLD signal response in the present study. That being said, contribution of behavioral state-change in BOLD signal fluctuation cannot be ruled out completely in the current study. Future investigation that realizes simultaneous Ca^{2+} imaging and optogenetic manipulation of neurons and/or astrocytes *in vivo* should deepen our understandings of the role of astrocytes on BOLD signal induction. In performing this experiment, sophisticated experimental setup would be necessary to avoid possible interference of excitation light for Ca^{2+} imaging on photocycle of ChR2(C128S).

Supplementary Discussion

AC is involved in many physiological effects, such as increased glucose metabolism (Ori, Freo, Pizzolato, & Dam, 2002), acetylcholine release (Imperato, Ramacci, & Angelucci, 1989), and cerebral blood flow in the brain (Postiglione et al., 1991). It is tempting to speculate that astrocyte-derived AC can be an energy substrate for neurons by fueling tricarboxylic acid (TCA) cycle in neurons because 1) acyl-carnitine including AC is known to facilitate influx and efflux of acetyl groups across the inner membrane of mitochondria, and 2) AC can be converted to neurotransmitters such as glutamate and GABA via TCA-cycle (Hadera et al., 2016; Jones, McDonald, & Borum, 2010; Scafidi et al., 2010). Additionally, it's noteworthy that co-occurrence of carnitine-decrease and AC-increase at the site of optogenetic astrocyte activation indicates *de novo* synthesis of AC in the brain upon astrocyte activation. AC has been considered to enter the brain through the blood-brain barrier via the high affinity, Na^{+}

232 dependent organic cation/carnitine transporters such as OCTN2, which is abundant on
233 astrocyte endfeet (Scafidi et al., 2010).

Supplementary References

Buzsáki, G., Buhl, D. L., Harris, K. D., Csicsvari, J., Czéh, B., & Morozov, A. (2003). Hippocampal network patterns of activity in the mouse. *Neuroscience*, *116* (1), 201–211. doi:10.1016/S0306-4522(02)00669-3

Carr, M. F., Karlsson, M. P., & Frank, L. M. (2012). Transient slow gamma synchrony underlies hippocampal memory replay. *Neuron*, *75* (4), 700–713. doi:10.1016/j.neuron.2012.06.014

Christie, I. N., Wells, J. A., Southern, P., Marina, N., Kasparov, S., Gourine, A. V., & Lythgoe, M. F. (2012). fMRI response to blue light delivery in the naïve brain: Implications for combined optogenetic fMRI studies. *NeuroImage*, *66* (1), 634–641. doi:10.1016/j.neuroimage.2012.10.074

Hadera, M. G., McDonald, T., Smeland, O. B., Meisingset, T. W., Eloqayli, H., Jaradat, S., … Sonnewald, U. (2016). Modification of Astrocyte Metabolism as an Approach to the Treatment of Epilepsy: Triheptanoin and Acetyl-L-Carnitine. *Neurochemical Research*, *41* (1–2), 86–95. doi:10.1007/s11064-015-1728-5

Imperato, A., Ramacci, M. T., & Angelucci, L. (1989). Acetyl-L-carnitine enhances acetylcholine release in the striatum and hippocampus of awake freely moving rats. *Neuroscience Letters*, *107* (1–3), 251–255.

Jones, L. L., McDonald, D. A., & Borum, P. R. (2010). Acylcarnitines: role in brain. *Progress in Lipid Research*, *49* (1), 61–75. doi:10.1016/j.plipres.2009.08.004

Kanemaru, K., Sekiya, H., Xu, M., Satoh, K., Kitajima, N., Yoshida, K., … Tanaka, K. F. (2014). In Vivo visualization of subtle, transient, and local activity of astrocytes using an ultrasensitive Ca2+ indicator. *Cell Reports*, *8* (1), 311–318. doi:10.1016/j.celrep.2014.05.056

Komaki, Y., Hikishima, K., Shibata, S., Konomi, T., Seki, F., Yamada, M., … Okano, H. (2016). Functional brain mapping using specific sensory-circuit stimulation and a theoretical graph network analysis in mice with neuropathic allodynia. *Scientific Reports*, *6*, 37802. doi:10.1038/srep37802

Mattis, J., Tye, K. M., Ferenczi, E. A., Ramakrishnan, C., O'Shea, D. J., Prakash, R., … Deisseroth, K. (2012). Principles for applying optogenetic tools derived from

direct comparative analysis of microbial opsins. *Nature Methods*, *9* (2), 159–172. doi:10.1038/nmeth.1808

Nagaoka, T., Zhao, F., Wang, P., Harel, N., Kennan, R. P., Ogawa, S., & Kim, S.-G. (2006). Increases in oxygen consumption without cerebral blood volume change during visual stimulation under hypotension condition. *Journal of Cerebral Blood Flow and Metabolism*, *26* (8), 1043–1051. doi:10.1038/sj.jcbfm.9600251

Nakamura, K. C., Kameda, H., Koshimizu, Y., Yanagawa, Y., & Kaneko, T. (2008). Production and histological application of affinity-purified antibodies to heat-denatured green fluorescent protein. *The Journal of Histochemistry and Cytochemistry*, *56* (7), 647–657. doi:10.1369/jhc.2008.950915

Nimmerjahn, A., Mukamel, E. A., & Schnitzer, M. J. (2009). Motor Behavior Activates Bergmann Glial Networks. *Neuron*, *62* (3), 400–412. doi:10.1016/j.neuron.2009.03.019

Ori, C., Freo, U., Pizzolato, G., & Dam, M. (2002). Effects of acetyl-l-carnitine on regional cerebral glucose metabolism in awake rats. *Brain Research*, *951* (2), 330–335. doi:10.1016/S0006-8993(02)03290-0

Paukert, M., Agarwal, A., Cha, J., Doze, V. A., Kang, J. U., & Bergles, D. E. (2014). Norepinephrine controls astroglial responsiveness to local circuit activity. *Neuron*, *82* (6), 1263–1270. doi:10.1016/j.neuron.2014.04.038

Postiglione, A., Soricelli, A., Cicerano, U., Mansi, L., De Chiara, S., Gallotta, G., … Salvatore, M. (1991). Effect of acute administration of l-acetyl carnitine on cerebral blood flow in patients with chronic cerebral infarct. *Pharmacological Research*, *23* (3), 241–246. doi:10.1016/S1043-6618(05)80083-0

Quiroga, R. Q., Nadasdy, Z., & Ben-Shaul, Y. (2004). Unsupervised spike detection and sorting with wavelets and superparamagnetic clustering. *Neural Computation*, *16* (8), 1661–1687. doi:10.1162/089976604774201631

Rungta, R. L., Osmanski, B.-F., Boido, D., Tanter, M., & Charpak, S. (2017). Light controls cerebral blood flow in naive animals. *Nature Communications*, *8*, 14191. doi:10.1038/ncomms14191

Scafidi, S., Fiskum, G., Lindauer, S. L., Bamford, P., Shi, D., Hopkins, I., & McKenna, M. C. (2010). Metabolism of acetyl-L-carnitine for energy and neurotransmitter

synthesis in the immature rat brain. *Journal of Neurochemistry*, *114* (3), 820–831. doi:10.1111/j.1471-4159.2010.06807.x

Schmid, F., Wachsmuth, L., Albers, F., Schwalm, M., Stroh, A., & Faber, C. (2016). True and apparent optogenetic BOLD fMRI signals. *Magnetic Resonance in Medicine*. doi:10.1002/mrm.26095

Song, X.-W., Dong, Z.-Y., Long, X.-Y., Li, S.-F., Zuo, X.-N., Zhu, C.-Z., … Zang, Y.-F. (2011). REST: a toolkit for resting-state functional magnetic resonance imaging data processing. *PloS One*, *6* (9), e25031. doi:10.1371/journal.pone.0025031

Srinivasan, R., Huang, B. S., Venugopal, S., Johnston, A. D., Chai, H., Zeng, H., … Khakh, B. S. (2015). Ca2+ signaling in astrocytes from Ip3r2-/- mice in brain slices and during startle responses in vivo. *Nature Neuroscience*, *18* (5), 708–717. doi:10.1038/nn.4001

Sugiura, Y., Honda, K., Kajimura, M., & Suematsu, M. (2014). Visualization and quantification of cerebral metabolic fluxes of glucose in awake mice. *Proteomics*, *14* (7–8), 829–838. doi:10.1002/pmic.201300047

Sugiura, Y., Honda, K., & Suematsu, M. (2015). Development of an Imaging Mass Spectrometry Technique for Visualizing Localized Cellular Signaling Mediators in Tissues. *Mass Spectrometry*, *4* (1), 1–9. doi:10.5702/massspectrometry.A0040

Sugiura, Y., Taguchi, R., & Setou, M. (2011). Visualization of spatiotemporal energy dynamics of hippocampal neurons by mass spectrometry during a kainate-induced seizure. *PloS One*, *6* (3), e17952. doi:10.1371/journal.pone.0017952

Takata, N., Shinohara, Y., Ohkura, M., Mishima, T., Nakai, J., & Hirase, H. (2014). Imaging of Astrocytic Activity in Living Rodents. *NeuroMethods*, *85*, 191–207.

Takata, N., Yoshida, K., Komaki, Y., Xu, M., Sakai, Y., Hikishima, K., … Tanaka, K. F. (2015). Optogenetic activation of CA1 pyramidal neurons at the dorsal and ventral hippocampus evokes distinct brain-wide responses revealed by mouse fMRI. *PloS One*, *10* (3), e0121417. doi:10.1371/journal.pone.0121417

Tanaka, K. F., Ahmari, S. E., Leonardo, E. D., Richardson-Jones, J. W., Budreck, E. C., Scheiffele, P., … Hen, R. (2010). Flexible Accelerated STOP Tetracycline Operator-knockin (FAST): a versatile and efficient new gene modulating system.

Biological Psychiatry, *67* (8), 770–773. doi:10.1016/j.biopsych.2009.12.020

Tanaka, K. F., Matsui, K., Sasaki, T., Sano, H., Sugio, S., Fan, K., … Yamanaka, A. (2012). Expanding the repertoire of optogenetically targeted cells with an enhanced gene expression system. *Cell Reports*, *2* (2), 397–406. doi:10.1016/j.celrep.2012.06.011

Tanaka, K. F., Takebayashi, H., Yamazaki, Y., Ono, K., Naruse, M., Iwasato, T., … Ikenaka, K. (2007). Murine model of Alexander disease: analysis of GFAP aggregate formation and its pathological significance. *Glia*, *55* (6), 617–631. doi:10.1002/glia.20486

Tsurugizawa, T., Ciobanu, L., & Le Bihan, D. (2013). Water diffusion in brain cortex closely tracks underlying neuronal activity. *Proceedings of the National Academy of Sciences of the United States of America*. doi:10.1073/pnas.1303178110

Yamamoto, H. A. (1992). Nitroprusside intoxication: protection of alpha-ketoglutarate and thiosulphate. *Food and Chemical Toxicology*, *30* (10), 887–890.

Yoshida, K., Mimura, Y., Ishihara, R., Nishida, H., Komaki, Y., Minakuchi, T., … Takata, N. (2016). Physiological effects of a habituation procedure for functional MRI in awake mice using a cryogenic radiofrequency probe. *Journal of Neuroscience Methods*, *274*, 38–48. doi:10.1016/j.jneumeth.2016.09.013

Supplementary Figure Legends

Supplementary Figure 1. Engineering of neuron-, astrocyte-, or ventral astrocyte-specific ChR2(C128S) mice.

(**a**) Gene manipulation strategies. Top, tetO cassette was inserted downstream of the Actb polyA signal in tetO knockin mice, but with no gene induction. Middle, tTA-mediated gene induction. tTA binds to the tTA-dependent promoter (tetO) and transactivates the transcription of ChR2(C128S) in double-transgenic mice. Bottom, The tetO cassette was removed by crossing with Cre mice, yielding Cre recombination. tetO, Tetracycline operator; tTA, tetracycline-controlled transcriptional activator; pA, polyadenylation signal; loxP, locus of X-over P1.

(**b**) Strategy for the generation of neuron-, astrocyte-, or ventral astrocyte-specific ChR2(C128S) mice. Neuron-ChR2 mice: *Chrm4*-tTA induced the expression of ChR2 in neurons, resulting in *Chrm4*-tTA::tetO-ChR2(C128S)-EYFP double-transgenic mice. Astrocyte-ChR2 mice: Mlc1-tTA induced the expression of ChR2 in astrocytes, resulting in Mlc1-tTA::tetO-ChR2(C128S)-EYFP double-transgenic mice. Astrocyte-ChR2 mice with Emx1-Cre: Mlc1-tTA induced the expression of ChR2 in astrocytes in ventral telencephalon (lower panel), but not in dorsal telencephalon by Cre-mediated removal of tetO cassette (upper panel). This results in *Emx1*-Cre; Mlc1-tTA::tetO-ChR2(C128S)-EYFP triple transgenic mice.

Supplementary Figure 2. Transcranial light illumination evoked BOLD signal response in the subcortical region of Astrocyte-ChR2 with *Emx1*-Cre.

(**a**) Left, Schematic expression pattern of *Emx1*-Cre (black area) in a coronal brain

section of *Emx1*-Cre mouse (Tanaka et al., 2007). Right, DAB immunohistochemistry against YFP (ChR2-marker) on coronal sections of the brain from Astrocyte-ChR2 with *Emx1*-Cre mice. This demonstrates a lack of ChR2(C128S) expression in the dorsal telencephalon. Scale bar: 1 mm. (**b**) A strategic diagram to generate *Emx1*-Cre; Mlc1-tTA::tetO-ChR2(C128S)-EYFP triple transgenic mice. (**c**) Transcranial light illumination of the brain from n = 2 Astrocyte-ChR2 with *Emx1*-Cre mice resulted in BOLD response at subcortical region (an arrow points at superior colliculus). This demonstrates that sufficient light reached through the skull to the subcortical region to activate the ultra-sensitive ChR2(C128S) (Mattis et al., 2012). (**d**) Time-course of BOLD signal fluctuation upon optogenetic activation of astrocytes at an arrow in (**c**). Blue and yellow vertical lines show timing of illumination for each color. (**e, f**) ofMRI using *anesthetized* Astrocyte-ChR2 mice (three measurements from 2 mice) demonstrated BOLD signal fluctuation upon optogenetic activation of astrocytes without behavioral response of mice. The duration of blue and yellow light was 0.5 s only in this observation. Medetomidine was used for anesthesia (Takata et al., 2015).

Supplementary Figure 3. BOLD signal fluctuation upon optogenetic stimulation of neurons or astrocytes with only yellow light or reduced power light.

(**a, b**) Time course of BOLD signal fluctuations in the cortex of n = 7 Neuron- (**a**) or n = 8 Astrocyte-ChR2 mice (**b**), upon illumination by pairs of yellow lights separated by 30 s. (**c, d**) Time courses of BOLD signal responses in the cortex of n = 13 Neuron- (**c**) or n = 11 Astrocyte-ChR2 mice (**d**), upon optogenetic activation using light power modulated to 10%, 20%, and 100% of that used in other experiments (i.e. Figs. 2–4). Grey shading indicates the SEM.

Supplementary Figure 4. Optogenetic stimulation of either neurons or astrocytes did not induce behavioral response.

(**a**) A photo of a freely moving mouse with an optical fiber attached on the surface of its skull. (**b**) Representative data of the tracking of the mouse position during a habituation period (8.5 min; Habituation) and a following period after habituation with light illumination (8.5 min; Light). Scale bar: 5 cm. (**c**) Representative locomotion velocity (black trace, left axis) and travel distance (gray trace, right axis) of a Neuron-ChR2 (left) or Astrocyte-ChR2 (right) mouse are plotted against time (bin width = 1 s). (**d**) Grouped data that compares mean velocity of 3 Neuron-ChR2 (left panel) or 3 Astrocyte-ChR2 (right panel) mice during the last 30 s of a habituation period, 30 s prior to the blue light illumination (Pre), and 30 s after the blue light illumination (Light). Mean velocity of mice was not modulated by light illumination (1.9 ± 0.1 versus 3.2 ± 1.4, P = 0.11 for Neuron-ChR2 mice, 1.2 ± 0.2 versus 1.3 ± 0.3, P = 0.61 for Astrocyte-ChR2 mice; paired *t*-test). Data are mean ± SD. NS: not significant.

Supplementary Figure 5. Electrophysiological response upon optogenetic stimulation of neurons or astrocytes with only yellow light or reduced power light.

(**a, b**) Time courses of LFP-power at each frequency band from n = 5 Neuron- (**a**) or n = 5 Astrocyte-ChR2 mice (**b**), upon illumination by pairs of yellow lights. Data are normalized (see methods). Vertical yellow lines indicate the delivery of yellow light pulses. (**c, d**) Relative number of MUA counts per 1.5-s bin, recorded at the most superficial 10 channels of the silicon probe electrode in the cortex of n = 5 Neuron-ChR2 (**c**) or n = 5 Astrocyte-ChR2 mice (**d**). (**e, f**) Time courses of LFP-power at each frequency

band from n = 6 Neuron- (**e**) or n = 5 Astrocyte-ChR2 mice (**f**), upon illumination by blue and yellow light, whose power was modulated as described in Supplementary Fig. 1. Data are normalized (see methods). Vertical blue and yellow lines indicate the delivery of light pulses of each color. (**g, h**) Relative number of MUA counts per 1.5-s bin, recorded at the most superficial 10 channels of the silicon probe electrode in the cortex of n = 6 Neuron- (**g**) or n = 5 Astrocyte-ChR2 mice (**h**). Gray shading indicates SEM which envelopes a mean trace.

Supplementary Figure 6. Representative images of other metabolites after optogenetic stimulation of astrocytes.

(**a**) Additional representative IMS images for AC/carnitine ratio (lower left) and $^{13}C_2$-AC/carnitine ratio (lower right) after optogenetic stimulation of the left cortex of an Astrocyte-ChR2 mouse. Upper images are optical images of a coronal brain section used for IMS. (**b**) Representative IMS images for glucose flux (left column), NADH (top panel at right column), and adenosine-nucleotides (bottom three panels at right column) after optogenetic stimulation of the cortex of the same Astrocyte-ChR2 mouse as Fig. 4d. Images (top to bottom, left to right) represent lactate, $^{13}C_2$-lactate, glutamate, $^{13}C_2$-glutamate, NADH, ATP, ADP, and AMP. Arrow heads in the panels indicate regions that showed significant increase of AC (Fig. 4d). Scale bar, 2 mm.

Supplementary Figure 7. AC-increase upon optogenetic stimulation of astrocytes demonstrated by CE/ESI/MS technique.

Amount of carnitine, AC, and $^{13}C_2$-AC in the dorsal cortexes that were ipsilateral and contralateral to the optical stimulation was compared (upper panel), using a CE/ESI/MS

technique that analyzed micro-dissected brain tissues from n = 3 Astrocyte-ChR2 mice. Amount of AC in the ipsilateral cortex was significantly higher than that in the contralateral cortex after optogenetic stimulation (*P = 0.04, paired *t*-test; lower middle). There was tendency of carnitine decrease (lower left) and $^{13}C_2$-AC increase (lower right) in the ipsilateral cortex (P = 0.54 for carnitine and P = 0.23 for $^{13}C_2$-AC, paired *t*-test). These results support the imaging observation by IMS (Fig. 4d).

Supplementary Figure 1

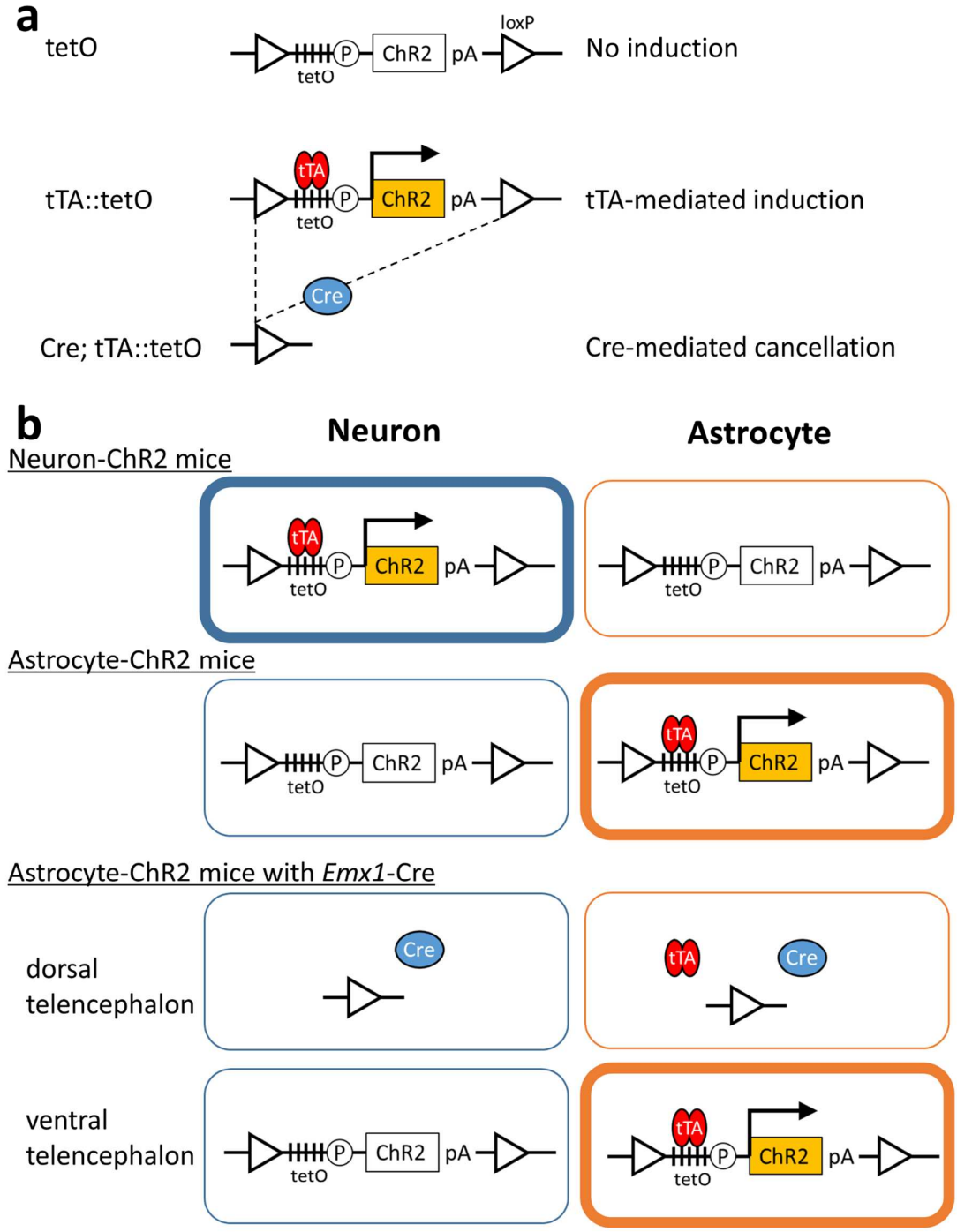

Supplementary Figure 2

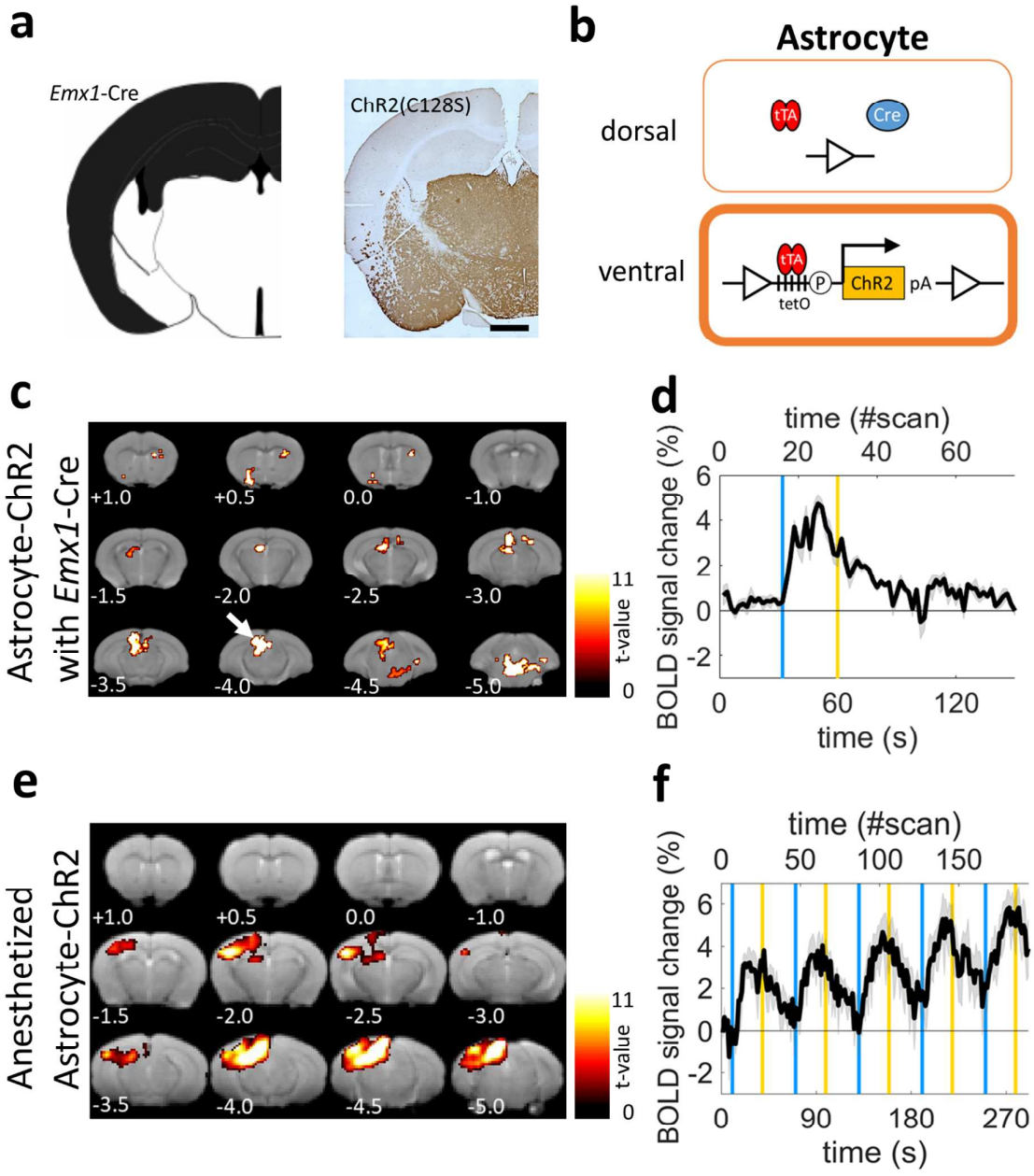

447

Supplementary Figure 3

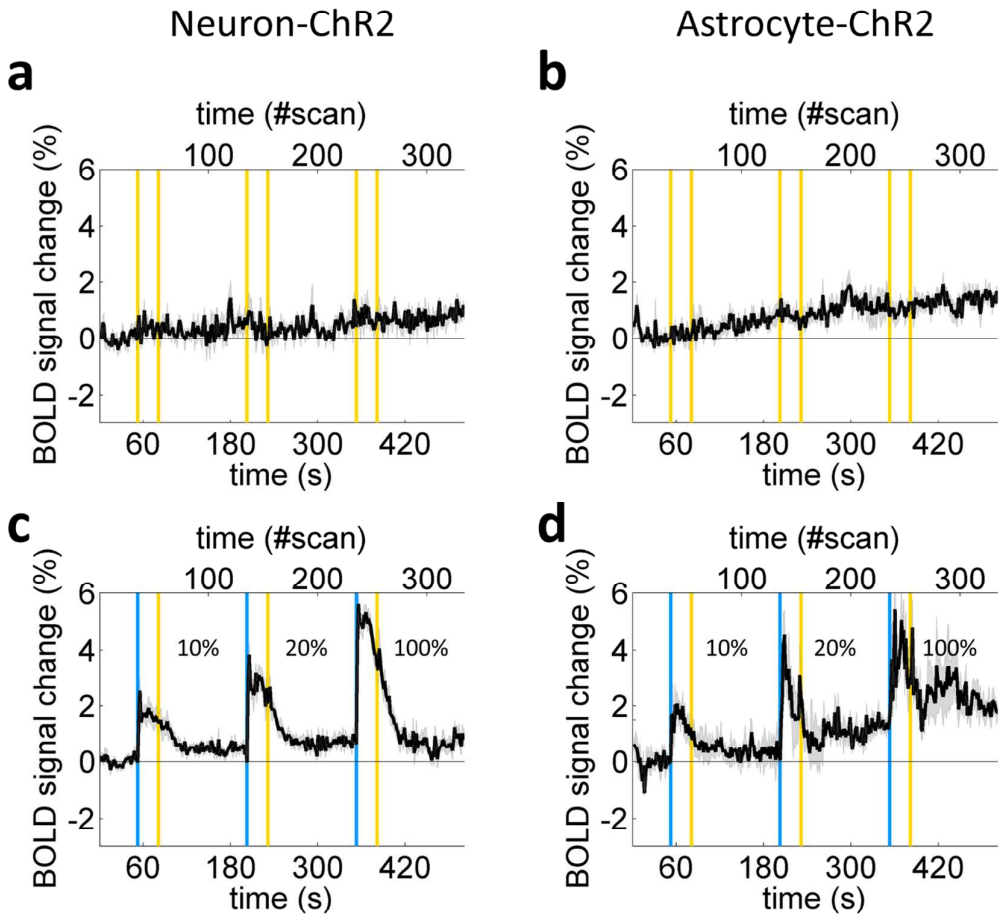

448

Supplementary Figure 4

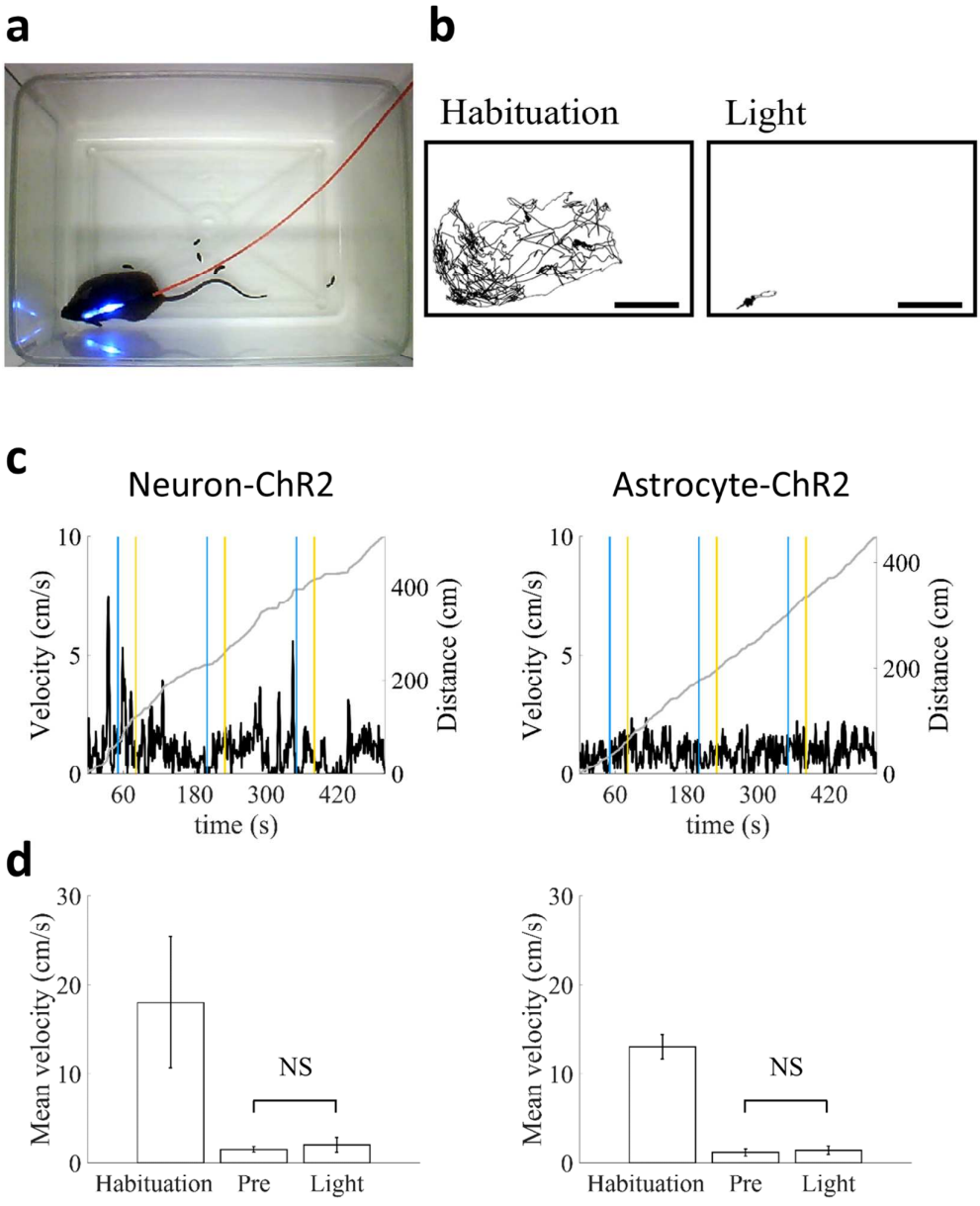

449

Supplementary Figure 5

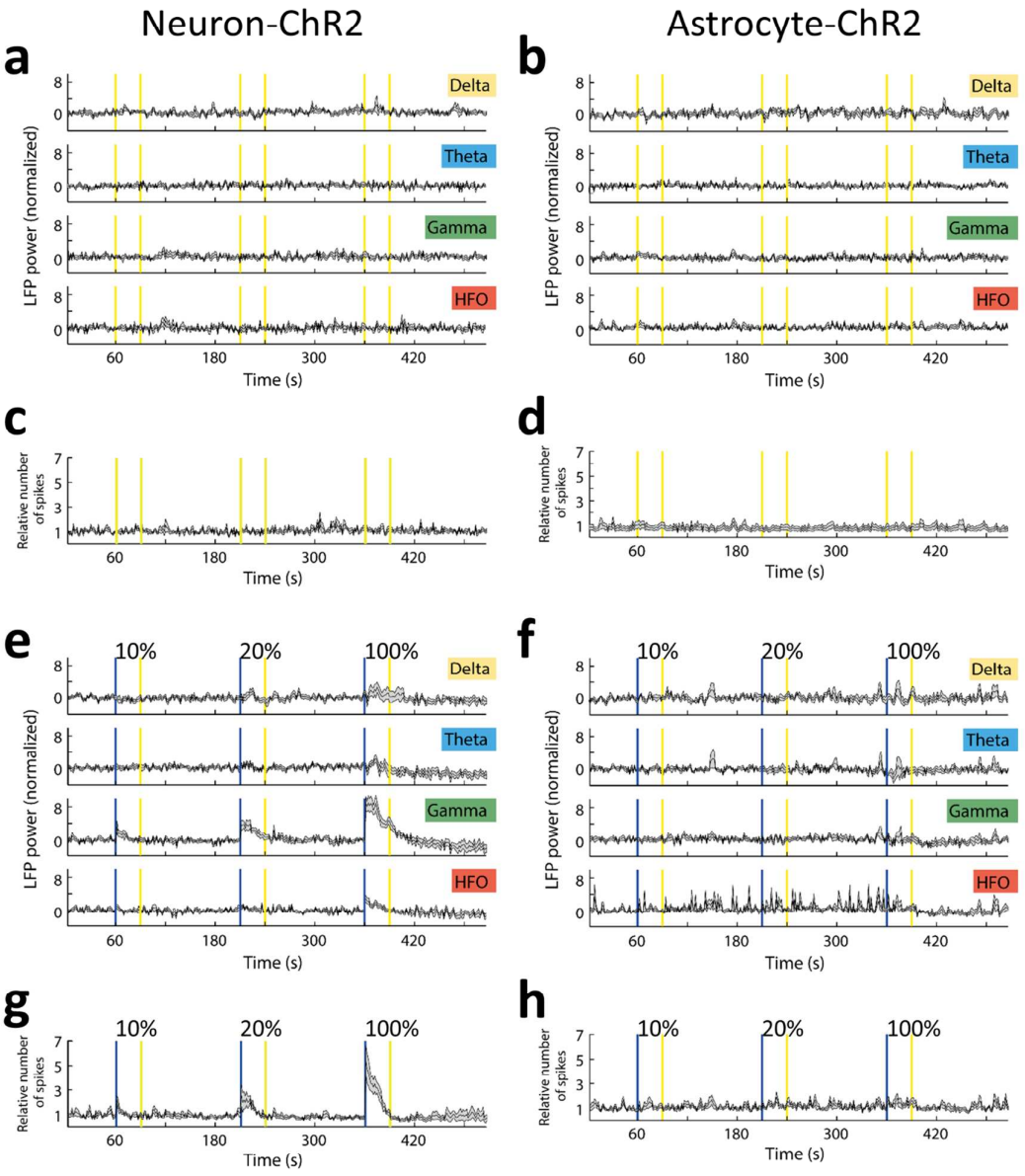

450

Supplementary Figure 6

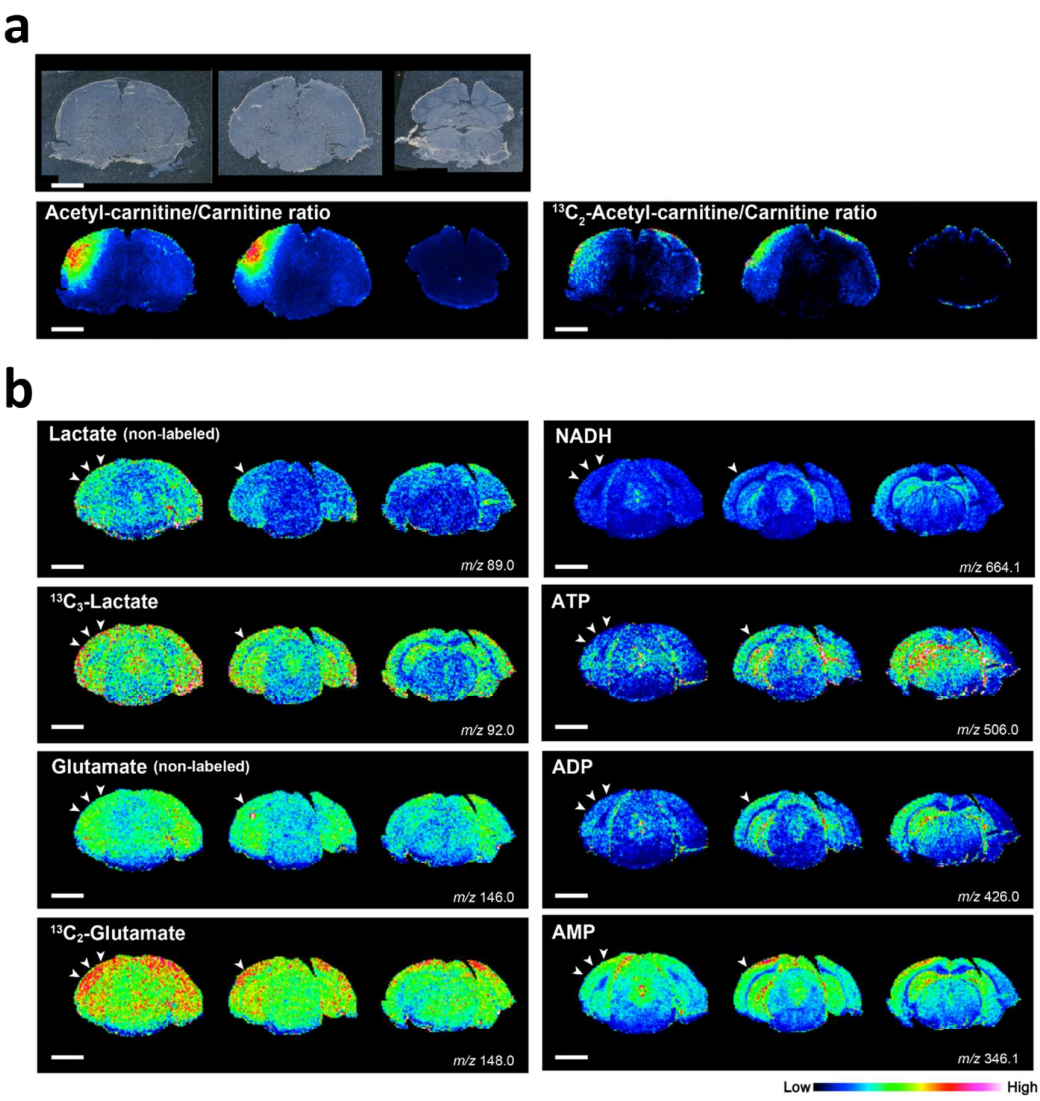

451

Supplementary Figure 7

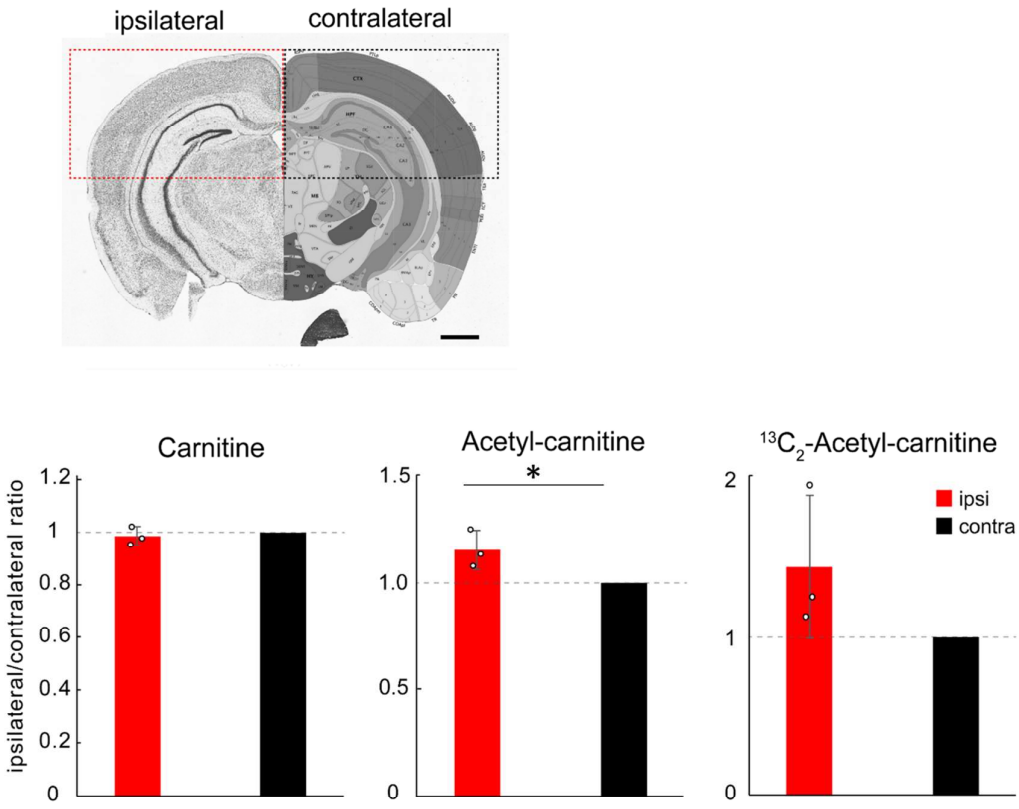

452